IEEE Access
Multidisciplinary ⋮ Rapid Review ⋮ Open Access Journal

Received January 29, 2021, accepted February 6, 2021, date of publication February 12, 2021, date of current version March 3, 2021.

*Digital Object Identifier 10.1109/ACCESS.2021.3058969*

# An Advanced Flexible Multiflow Path Fixture Cooling Method for Additive Manufacturing Repair of Aero Blades

**MIAO GONG[1,2], SHIJIE DAI[1], LIWEN WANG[2], AND TAO WANG[2]**
[1]School of Mechanical Engineering, Hebei University of Technology, Tianjin 300041, China
[2]Institute of Aviation Engineering, Civil Aviation University of China, Tianjin 300300, China

Corresponding author: Miao Gong (mgong69@163.com)

This work was supported in part by the National Key R&D Program of China under Grant 2019YFB1311100, in part by the Special Fund for the Central Government to Guide the Development of Local Science and Technology under Grant 19941603G, and in part by the Joint Fund for Civil Aviation of China under Grant U1633104.

**ABSTRACT** Currently, how to release the heat accumulated in the molten pool rapidly is the key factor in blade repair. We analyzed the problem of the current cooling method in blade additive manufacturing repair. Based on cooling effect, we proposed an advanced flexible multiflow path fixture cooling method for blade additive manufacturing repair. We created a coupled heat transfer model and deduced the heat transfer law for multiflow path conjugate flexible clamping. We obtained the optimal cooling scheme for flexible multiflow paths through numerical analysis. We built an experimental platform and tested the cooling effect of the fixture prototype by experiment. The results show that compared with the current cooling method, the new cooling method not only can lower the initial temperature of the fixture rapidly and realize the steady-state heat transfer between the fixture and the flow path quickly but can also significantly enhance the ability of fluid to participate in heat transfer in new flow paths, which significantly improves the cooling effect. The research results are of great significance for the improvement of aero blade additive manufacturing repair.

**INDEX TERMS** Cooling method, blade repair, flexible fixture, numerical analysis, heat transfer.

## I. INTRODUCTION

In additive manufacturing repair of aviation compressor blades, the heat accumulation in the molten pool usually reduces the repair quality of the blades. Under the condition of effective heat input, how to release the heat accumulated in the molten pool rapidly is the key factor in blade repair. Currently, the fixture base cooling method with a single flow path is widely used in civil aviation maintenance, and it can achieve an effect when a single material with low additive height (less than 1 mm) is added [1]. However, it is difficult to achieve better repair quality with a second additive manufacturing repair or larger additive manufacturing height due to the increased cooling requirements.

Additive manufacturing repair of compressor blades is mainly aimed at 4∼9 stage blades, which are ultrathin alloys with very small volumes. The repair is a kind of high standard surface welding. The fluid flow should be considered in addition to the overall heat transfer characteristics [2], [3]. Forced cooling of fluid is an effective cooling method in welding, which mainly includes air jet impact cooling [4], liquid gas cooling and water cooling.

On the research of liquid gas cooling in welding, liquid $CO_2$ cooling and liquid $N_2$ cooling are widely used. The distortion and longitudinal residual stress of weldment can be greatly reduced by liquid $CO_2$ cooling [5]. Murhid *et al.* [6] studied the post-weld mechanical properties of carbon steel friction stir welding and the relationship between the microstructure and the cooling rate, and they pointed out that, compared with natural cooling, rapid cooling with liquid $CO_2$ enhanced the mechanical properties of the welded joints. Hideki *et al.* [7] used two kinds of liquid $N_2$ cooling methods to cool laser-welded ultrafine grain steel, and they analyzed its effect on the size of the heat-affected zone. Method 1 fixed the welded specimen in static liquid nitrogen through a fixture; method 2 fixed the test piece on the liquid nitrogen channel and analyzed the influence of the liquid nitrogen depth and the initial temperature on the

The associate editor coordinating the review of this manuscript and approving it for publication was Jesus Felez.

heat-affected zone. Manikandan *et al.* [8] designed a method to process the flow channel in the welding pad and introduce liquid nitrogen to cool the TIG welding process of nickel base alloy. They studied the effect of liquid nitrogen flow rate on the formation of interdendritic Laves phase [9] and pointed out that forced cooling method could effectively reduce the generation of Laves phase but the inflow rate and boiling rate of liquid $N_2$ is difficult to balance. In the process of liquid gas cooling, the controllability of the cooling rate and the uniformity of fixture temperature need to improve due to the fast flow rate and local supercooling.

On the research of water cooling in welding, Perret and Biswal [10] proposed an optimized radiator structure based on a theoretical model and performed experimental verification, the optimization results are in good agreement with the experimental data, and they obtained a rapid design and optimization method for a water-cooled radiator. J. Guisheng *et al.* [11] designed and optimized a kind of plate water-cooled radiator by using the unified dimensional method, and achieved good cooling effect. S. Shixuan *et al.* [12] set four cooling conditions: natural cooling, air cooling, atomizing water cooling and underwater cooling, and then, they analyzed the welding effect under different cooling conditions through comparative experiments. Shi Kangling *et al.* [13] designed a water cooling structure of the base plate at the bottom of the weld and adopted a forced cooling method by passing water into the flow channel after welding. Fan feiwen *et al.* [14] proposed a new water cooling system based on K-TIG welding by setting a cooling channel under the welding table. The principle of this method is comparable to that of Ref. [8] and Ref. [20]. The cooling medium is introduced into the copper plate under the workpiece, and the forced cooling of the fluid is used to cool the copper plate, so as to increase the temperature difference between the copper plate and the workpiece. The experimental results show that the width of weld and the volume of the molten pool can be significantly reduced by using this cooling system structure. Wen Peng *et al.* [15] used the dynamic back cooling method with cooling water as the medium to control the instability and deformation of the thin plate during laser welding. The optimal cooling parameters were obtained by optimizing the distance between the cold and heat sources and the flow rate of the cooling water. The experimental results showed that when the number of copper blocks in the fixture is increased to 8 and auxiliary cooling is used, the deformation of the thin plate is at the minimum.

Spray cooling is an effective cooling method in the field of aerospace [16], [17]. JiXiang Wang, *et al.* [18] developed a novel fluidic organization to realize the application of an airoriented spray cooling system. They developed design procedures of the ejector, fabricated a practical ejector and optimized the state of the input high-pressure air and water which is used to generate the spray flow according to the cooling performance, attained basic thermal laws regarding the gas-atomized spray cooling. On the basis of the research of Ref. [18], they also provide a ground-based experimental investigation of the gas-atomized spray cooling using various micro-structured surfaces and a flat surface [19]. They organized a comparison of spray cooling performances using the gas-atomized nozzle and pressure nozzle and point out that the gas-atomized spray cooling possesses a huge superiority where a heat transfer coefficient can be enhanced by 234%. Sun Jiamin *et al.* [20] studied the temperature field of electroslag welding joints under three cooling conditions, such as air cooling, copper cooling and spray cooling. Through the simulation calculation of the temperature field of the characteristic point, the thermal cycle curve of the characteristic point and the residence time above the phase transition temperature under three cooling modes are given. However, for welding, because of the divergence of the fluid and the scattering degree between the fluid and the contact surface, there will be a large deviation between the fluid properties and the simulation calculation, so the cooling speed is difficult to measure accurately.

In addition, Numerical analysis and computational fluid dynamics (CFD) are necessary means to study fluid cooling. Imane Khalil *et al.* [21] proposed a three-dimensional numerical simulation to quantify the design specifications of a heat exchanger (heat sink) with the directional channel of heat plate expansion. The results of the CFD simulation showed that the heat transfer performance of a heat plate is improved under various conditions, and the correctness of the model was verified by the experimental results. Marcin Sosnowski *et al.* [22] investigated the possibility of implementing an innovative multidisc sorption bed combined with a heat exchanger into adsorption cooling technology experimentally and numerically, and they incorporated a sorption model developed in-house into the commercial CFD code in the analysis [23].

The compressor blade of a new CFM56 series engine uses ultrathin alloys with a partial tip thickness of less than 1.5 mm. The two main repair methods currently used are Micro plasma arc welding (MPAW) surfacing and laser cladding [24]–[26]. Compare with laser cladding, MPAW is a low-cost metal joining technique for ultrathin alloy due to its inherent ability to control a constricted arc with low amperage current [27], [28]. However, due to the structure of current fixture, heat conduction distance between clamping contact surface and the fluid is long, how to improve the cooling effect is a key problem worthy of study in MPAW blade repair.

In order to achieve better cooling effect, this paper, on the basis of our previous study in optimal heat input [29], [30], an advanced flexible multiflow path fixture cooling method for additive manufacturing repair of aero blades was proposed according to the characteristics of MPAW blade repair. In Section 2, the problem of current cooling method was analyzed through numerical analysis. Then, the design of a flexible multiflow path fixture was introduced in Section 3 and the cooling effect of the new method was calculated by modeling and simulation in Section 4. The cooling effect was verified by experimental prototype in Section 5.

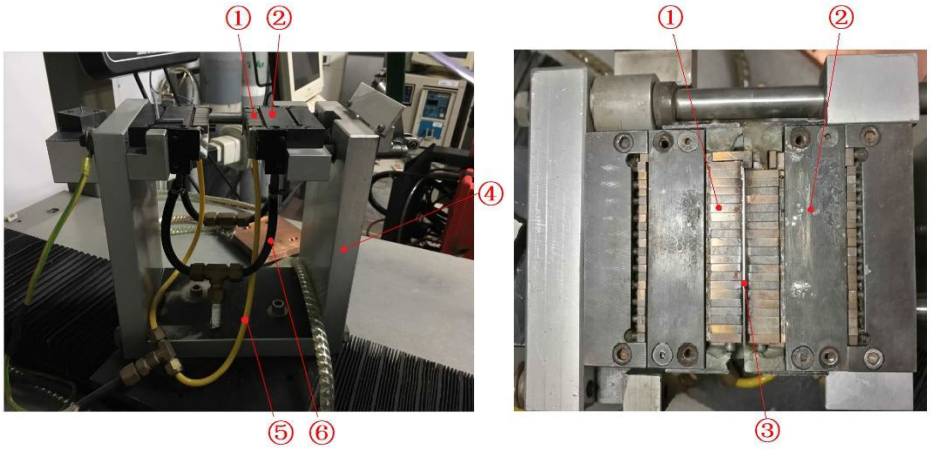


**FIGURE 1.** MPAW repair fixture: ① Movable copper bonds. ② Clamping structure. ③ Welding test piece. ④ Aluminum frame. ⑤ Protective gas pipeline. ⑥ Coolant pipeline.

The research is of great significance for the improvement of blade additive manufacturing repair technology in aviation maintenance.

## II. PROBLEM ANALYSIS OF THE FIXTURE BASE COOLING METHOD

### A. FINITE ELEMENT MODEL OF THE HEAT TRANSFER STRUCTURE

Currently widely used structure of the fixture base cooling method is shown in Figure 1. It is mainly composed of a copper heat-dissipating clamping structure and an aluminum frame. Two groups of horizontally movable copper bonds, similar to piano keys, are mounted on the clamping structure. Since the heat dissipation is mainly concentrated on the portion of the copper fixture that is close to the clamping surface, the model design considered only the copper clamping structure to simplify the calculation. Considering that the partial curvature of the blade clamp is small, in this study, a 1-mm-thick Inconel718 alloy rectangular sheet was used to simulate the compressor blade. The size of the alloy specimen is 65 mm×30 mm×1 mm. Since the fixture is a symmetrical structure, to simplify the calculation, one-half of the section of the test piece is taken as the plane of symmetry, and a finite element model is established; the meshing and mass distribution are shown in Figure 2.

A dense mesh was applied to the upper surface of the test piece and the front and upper ends of the copper bond, and a loose mesh was applied to the remainder. The grid contains 215,852 units, of which the smallest unit size is $1.79 \times 10^{-5}$ m, the maximum unit size is 0.00179 m, the maximum unit growth rate is 1.3, and the average grid quality is 0.6522. Based on this mesh generation, fluid mesh generation is added, and five layers of boundary layer mesh are applied to the wall surface of the fluid that contacts the fixture, with a stretch factor of 1.2 and a thickness adjustment factor of 1. The boundary layer mesh generation is shown in Figure 2(c).

### B. WALL FUNCTION AND FLUID BOUNDARY CONDITIONS

The design domain is located at the distance $\delta w$ from the wall:

$$\delta_w^+ = \rho u_\tau \delta_w / \mu \tag{1}$$

where $u_\tau = C_\mu^{1/4}\sqrt{k}$ is the friction velocity, which is equivalent to the distance between the logarithmic layer and the viscous sublayer, with a value of 11.06. The boundary conditions and the shear stress conditions of the velocity are shown in equations (2) ∼(5):

$$\mathbf{u} \cdot \mathbf{n} = 0 \tag{2}$$

$$\mathbf{n} \cdot \sigma - (\mathbf{n} \cdot \sigma \cdot \mathbf{n})\mathbf{n} = -\rho u_\tau \frac{\mathbf{u}}{u^+} \tag{3}$$

$$\sigma = \mu \left(\nabla \mathbf{u} + (\nabla \mathbf{u})^T\right) \tag{4}$$

$$u_\tau = \max\left(\frac{|\mathbf{u}|}{\frac{1}{\kappa_v}\ln \delta_w^+ + \mathrm{B}}, C_\mu^{1/4}\sqrt{k}\right) \tag{5}$$

where $\sigma$ is the viscous stress tensor, $\kappa_v$ is the Karman constant (the default value is 0.41), and B is the constant with a default value of 5.2. The turbulent kinetic energy obeys the uniform Neumann condition $\mathbf{n} \cdot \nabla k = 0$, and the boundary conditions of $\varepsilon$ is as follows:

$$\varepsilon = \frac{C_\mu^{3/4} k^{3/2}}{\kappa_v \delta_w} \tag{6}$$

Then, the fluid boundary conditions of the model are set as follows:

(1) Tap water with a temperature of 10 °C is used as an incompressible fluid;

(2) The right side of the channel is the inlet of the flow, and the velocity boundary conditions are applied to convert four kinds of velocity into the normal velocity of the flow to the cross-section;

(3) The left end of the flow channel is the outlet, and the pressure boundary condition is adopted. The outlet pressure is set at 0 Pa to restrain the reflux;

(4) The wall boundary condition is set to not slip.

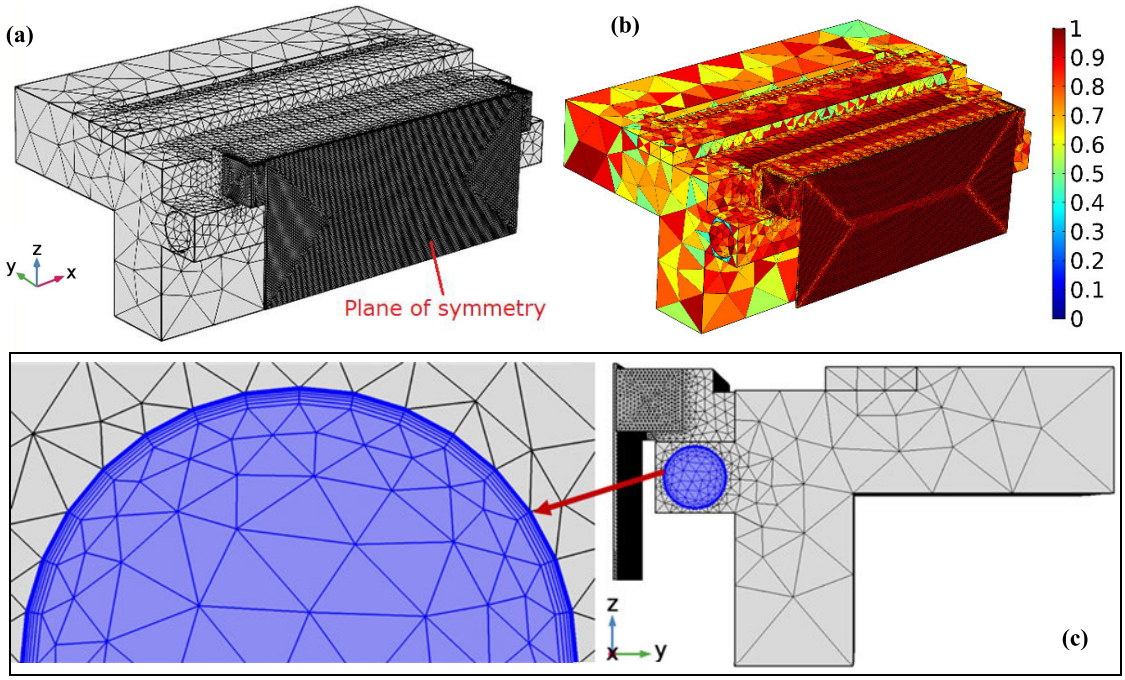


**FIGURE 2.** Meshing and mass distribution: (a) Finite element mesh generation and symmetry surface. (b) Mesh quality. (c) Boundary layer mesh generation.

### C. PROBLEM ANALYSIS

The sectional view of the base cooling fixture is shown in Figure 3. To analyze the cooling problem of the fixture base cooling method accurately, three groups of simulation experiments were set up. The cooling time and heat taken away were calculated with the change in parameters.

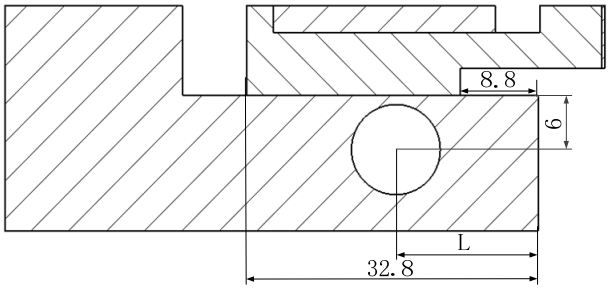


**FIGURE 3.** Sectional view of the base cooling fixture.

The simulation scheme is shown in Table 1, where $V$ is the flow rate of the cooling water, $T$ is the inflow temperature, $L$ is the horizontal distance between the flow path center and the base edge, $t$ is the cooling time (represents the time when the temperature rises from 650 K to the highest temperature and then drops to 650 K) of the middle position of the welding surface, $Q$ is the average heat carried away by cooling water per second in cooling time $t$.

The first group of simulations analyzes the influence of different cooling water flow rates $V$ on the cooling effect of weldments, and the results are shown in Figure 4. From the

**TABLE 1.** Three simulation schemes.

| NO. | $L$ (mm) | $T$ (°C) | $V$ (L/min) |
|---|---|---|---|
| 1 | 16 | 10 | 0.5, 1, 1.5, 2, 2.5, 3, 3.5, 4, 4.5, 5, 5.5 |
| 2 | 16 | 0, 2.5, 5, 7.5 10 | 5 |
| 3 | 12, 14, 16, 18, 20 | 10 | 5 |

laminar flow to turbulent flow, $t$ decreases with the increase in $V$, $Q$ increases with the increase in $V$, and the trend is gradually steeper and then slower. The convective heat transfer effect is stronger in turbulent flow than in laminar flow because internal particles always move in a straight line along the flow direction. The particles or flow layers are not mixed with each other. In turbulent flow, particles not only move along the flow direction but also move perpendicular to the flow direction. The particles or flow layers are mixed with each other, which increases the heat transfer between the cooling water. Compared with $V = 0.5$ L/min, $t$ is shortened by 0.186 s at $V = 5$ L/min, the decrease rate is 5.25%, and $Q$ is increased by 8.1274 J. However, $t$ and $Q$ tend to be stable with an increase in $V$ in turbulent flow. When $V$ is 5.0 L/min and 5.5 L/min, $t$ and $Q$ are 3.542 s, 3.540 s and 41.0478 J, 41.1164 J, respectively, with little change.

The second group of simulations analyzes the influence of different cooling water inflow temperatures on the cooling effect of weldment. The results are shown in Figure 5. The cooling water inflow temperature $T$ is gradually reduced,

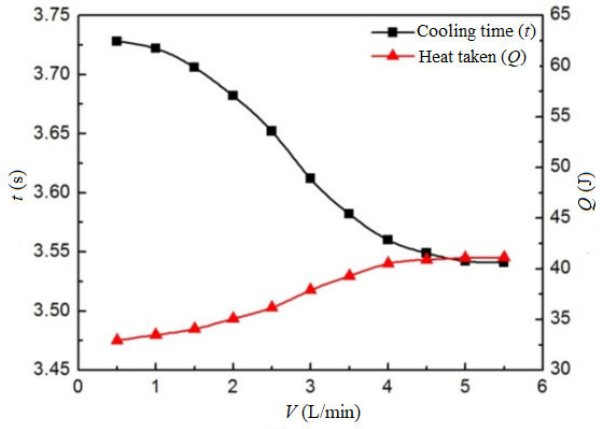


**FIGURE 4.** Cooling time and heat taken under different flow rates.

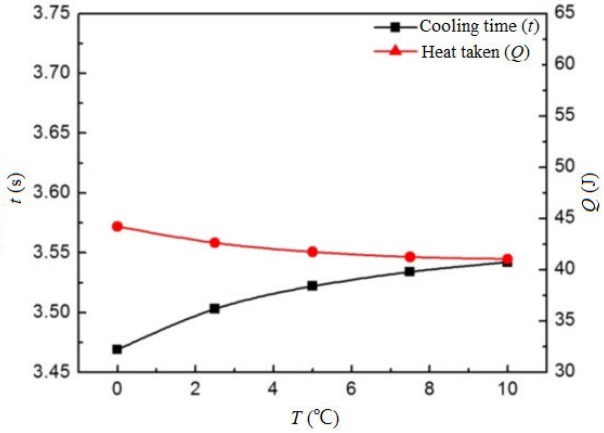


**FIGURE 5.** Cooling time and heat taken under different fluid temperatures.

from 10 °C to 0 °C, and there is no significant change in $T$ or $Q$. Although $Q$ increases gradually with the decrease in $T$, the increment is very small. It can be seen that the fluid has completely flowed out of the fixture flow path without sufficient heat exchange with the flow path wall. At 10 °C and 0 °C, $t$ and $Q$ are 3.542 s, 3.469 s and 41.0479 J, 44.2251 J, respectively. The cooling time $t$ is shortened by only 0.073 s, the shortening range was 2.06%, and $Q$ is increased by only 3.1774 J.

The third group of simulations analyzes the effect of different flow channel horizontal positions on the cooling effect of the weldments. We assume that the distance between the flow path and the lower surface of the copper bond is 1 mm and changes the horizontal position of the flow path. The results are shown in Figure 6. The flow path is located in multiple horizontal positions, but $T$ and $Q$ show no obvious change with $L$. The maximum and minimum values of $T$ are 3.548 s and 3.541 s, respectively, with a change range of 0.20%. The maximum and minimum values of $Q$ are 41.27 J and 39.83 J, respectively, and the difference is only 1.44 J. It can be seen

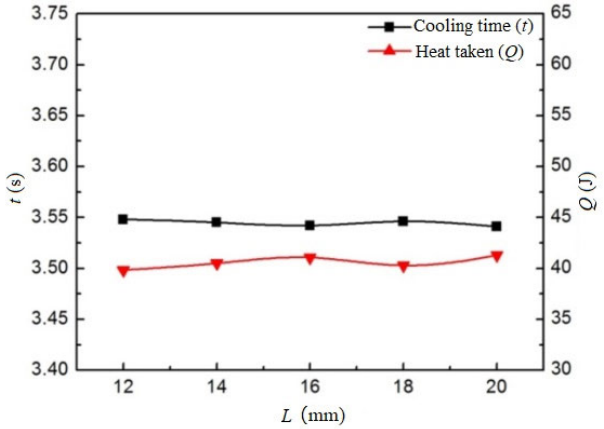


**FIGURE 6.** Cooling time and heat taken under different *Ls*.

that the change in $L$ has little effect on improving the cooling effect.

These simulation results show that regardless of whether $V$, $T$ or $L$ is changed, the cooling effect does not change significantly. Due to the original structural limitations of the fixture, the vertical distance between the heat source and the fluid is relatively long, and as a result, the heat exchange effect of the fluid is not fully utilized. In addition, in the actual clamping, there are still gaps between the copper bonds and the base of the fixture, which also affect the cooling effect.

After welding several times, the initial temperature of the fixture reaches temperatures above 70 °C. Figure 7 shows the heat conduction process of the copper bond under the fixture base cooling method at the initial temperature of 70 °C. The simulation results show that the time of the fluid cooling intervention is relatively late. In the first 4 s, the copper bond is mainly undergoing natural cooling, and then, the fluid heat exchange begins to intervene slowly, but the cooling rate of the copper bond is still slow. From the direction of the heat transfer, enhancing the heat conduction of the copper bond in the $y$-$z$ section is helpful for increasing the heat transfer efficiency.

## III. DESIGN OF A FLEXIBLE MULTIFLOW PATH FIXTURE

Since the original fixture base is closely related to the coordinate positioning and control of the MPAW system, the copper bond design scheme of the flexible multiflow path fixture keeps the original length of 43 mm unchanged. In addition, the total width of all of the copper bonds is consistent with the original fixture copper bonds, such that the original copper bonds can be replaced, and new copper bonds can be directly loaded on the original fixture base. Considering that when clamping a larger blade the curvature of the blade tip after clamping is smaller, the height and width of the copper bond are appropriately increased such that there is sufficient space inside the copper bond to accommodate the flow path. Therefore, the copper bond of the fixture not only maintains the original flexible clamping function but can also realize the

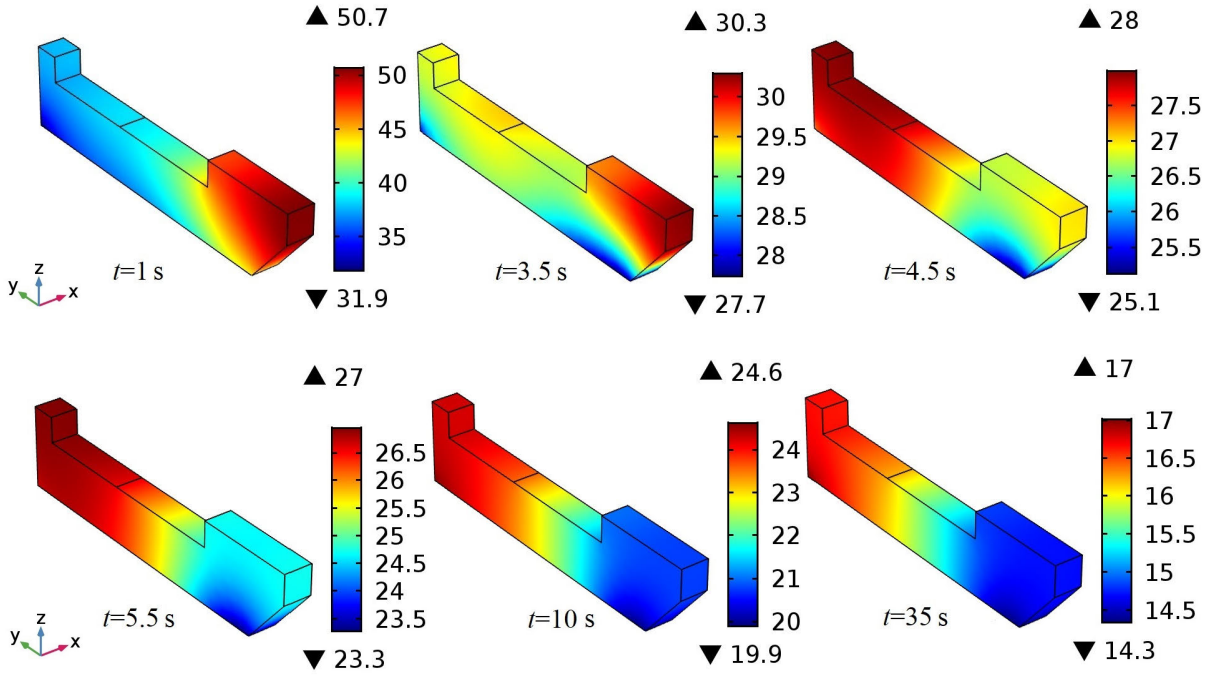


**FIGURE 7.** The heat conduction process of the copper bond under the fixture base cooling method with a single flow path.

purpose of active turbulent heat exchange in the flow path. In addition, the integrated design of the flow path and the copper bond greatly reduces the distance between the cooling fluid and the main heat dissipation clamping surface under this solution, thereby achieving better heat dissipation.

The three-dimensional model of the new structure of the fixture is shown in Figure 8. Eight movable copper bonds are installed on the base of each side of the fixture. To avoid the influence of the heat source on the temperature of the inflow fluid, the side of the flow channel opening near the test piece is set as the fluid outlet, and the other side, farther from the test piece, is the fluid inlet. In addition, to facilitate the installation of the cooling pipeline, the design inlet is 3 mm higher than the outlet.

The size and internal structure of the copper bond are shown in Figure 9. Considering the assembly precision and structural strength of the copper bonds of the fixture, the thickness of the copper bonds is designed to be 8 mm, and the diameter of the inner flow path of the copper bond is designed to be 3 mm; as a result, the thinnest part of the copper bond is greater than 2 mm. The height of the contact surface between the copper bond and the fixture is designed to be 3.5 mm, and the contact area reaches 28 mm$^2$. In the design of the internal flow path route, the principle of the optimal heat dissipation effect is followed, which enables the wall of the flow path to be as close as possible to the front clamping surface, and the nearest distance can be up to 3 mm.

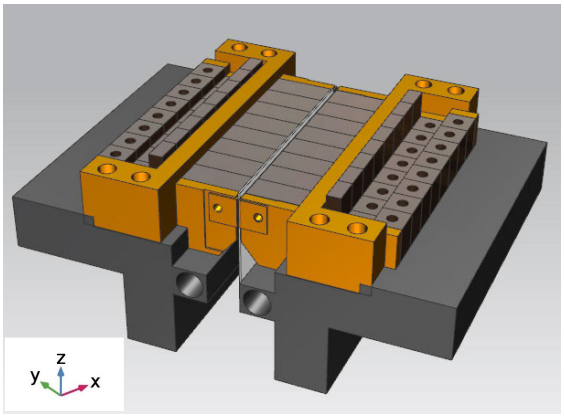


**FIGURE 8.** Three-dimensional model of the new structure of the flexible multiflow path fixture.

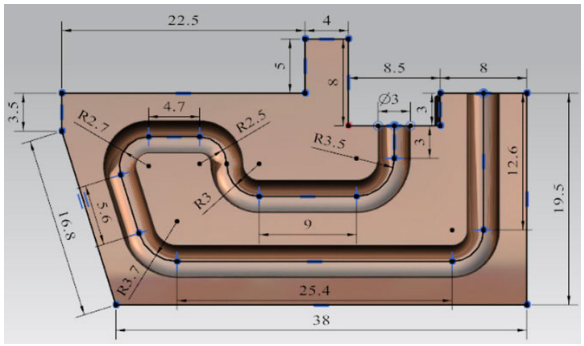


**FIGURE 9.** Outline dimension of copper bond and schematic diagram of runner structure.

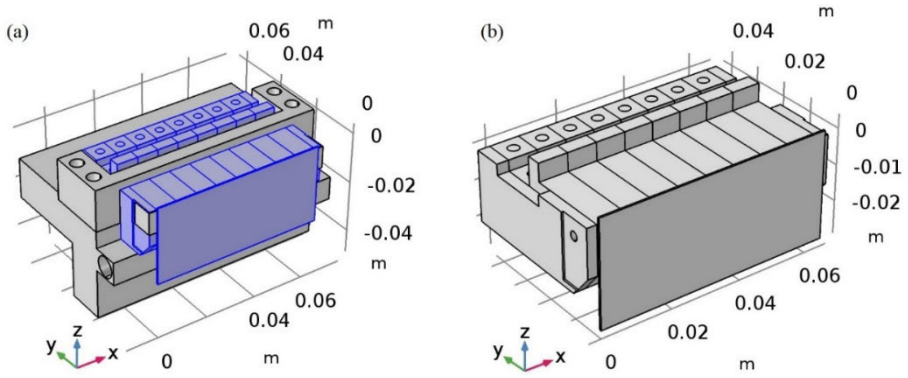


**FIGURE 10.** (a) Clip specific symmetry model; (b) Simplified model of key heat transfer part.

The total length of the flow path in the copper bond is 88.9 mm, the longest straight pipe length is 25.4 mm, and the second length is 12.4 mm; these are located in the first two sections of the inlet. After flowing into the copper bond through the inlet, the fluid immediately reaches the position that is closest to the contact surface after passing through the two longest straight pipes and two turns.

## IV. MODELING AND NUMERICAL ANALYSIS

### A. SIMPLIFIED MODEL OF THE FLEXIBLE MULTIFLOW PATH FIXTURE

One-half of the cross-section of the test piece is taken as a symmetrical plane, and a symmetrical model of the clamped half is established in COMSOL, as shown in Figure 10(a). We have carried out previous research of thermal resistance in welding [31], which is indeed a complex problem worth studying. This paper, we mainly propose a new cooling method and study the cooling effect. For the current fixture and the new fixture, when the clamping parts are the same, the cooling effect mainly depends on the cooling structure of the fixture itself. Moreover, the volume and curvature of compressor blades (mainly maintenance stages 4∼9) is small. Therefore, in order to simplify the calculation, the rectangular alloy sheet is used for modeling and analysis.

According to the analysis of the heat conduction mechanism of the fixture in previous research [4], the heat exchange is mainly concentrated between the test piece and the copper bond. The rear of the copper bond and the specific base and cover of the fixture have little effect on the heat dissipation process. Therefore, in order to reduce the number of grids and calculation, the base and the cover plate are removed, and the copper bonds and test pieces are taken as the research objects to establish a simplified heat transfer model. The research in this work is mainly based on the simplified heat transfer model shown in Figure 10(b).

### B. MESH GENERATION IN DIFFERENT STAGES OF FINDING THE SOLUTION

In design that uses flexible flow paths, the model becomes a coupling model of turbulent flow and solid heat transfer with multiple flow paths conjugated because the flow paths are distributed inside the copper bonds. If there is a very fine grid, even in the simplified model shown in Figure 10(b), the overall number of units will be close to 10 million, which will cause the need for an enormous number of calculations and very high computer hardware requirements, and it will also increase the probability of nonconvergence. To reduce the number of calculations and improve the convergence of the calculation results, the simplified fixture model was divided into two stages for targeted meshing, and then solved separately.

The first stage allows the fixture to establish a stable cooling cycle before the welding heat source is loaded, which can be called the precooling stage of the copper bonds. At this stage, the fluid through a turbulent heat exchange reduces the initial temperature of the copper bond of the fixture and forms a cooling cycle. The initial temperature of the fixture can be room temperature or a higher temperature after multiple welding. This heat transfer stage can be defined as the precooling stage. For the solution in the precooling stage, the three copper bonds in the middle of the fixture are taken as the main research objects, and the free tetrahedron mesh is used for the fine divisions. Since the thermal conductivity of the red copper is uniform, it is assumed that the density of the red copper bonds is uniform during the processing, the remaining copper bonds are divided using conventional grid accuracy. Because the heat source has not been loaded, the test piece is not the main thermally conductive solid at this stage. Therefore, the test piece is also meshed with conventional precision at this stage. The baffle plates on both sides show weak heat conduction and can be divided using a coarse mesh. The first stage of meshing is shown in Figure 11. For the flow paths in the copper bond, a boundary layer grid is used; the number of boundary layers is set to 5, the stretch factor is 1.2, and the copper bond is hidden. The grid division of the flow paths is shown in Figure 12.

The start of the welding can be regarded as the second stage of heat transfer, which can be called the welding heat transfer stage. At this stage, a high-density heat source is loaded on the upper surface of the test piece, and heat is transferred

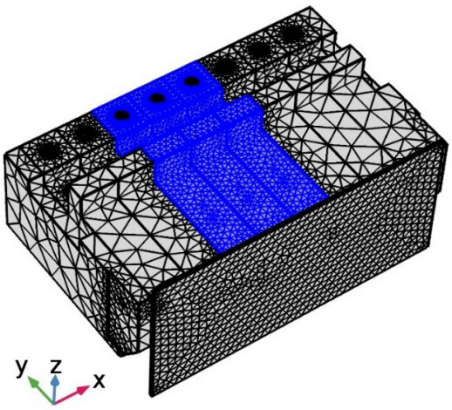


**FIGURE 11.** Mesh generation in the first stage of heat transfer.

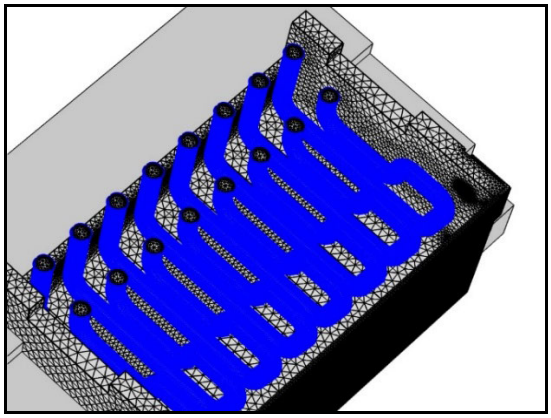

**FIGURE 12.** Mesh generation of the fluid boundary layer.

downward from the upper surface of the test piece along the $z$-$x$ plane. Since the thermal conductivity of the nickel-based alloy is lower than that of copper, the heat quickly expands to the $y$-$z$ plane after reaching the copper bond contact surface, and it continues to produce a large temperature difference with the fluid at a distance of 3 mm; the heat will be quickly conducted in the direction of the fluid. In the second stage, the main conduction surface of the heat is the contact surface of the copper bond with the fixture and the part of the test piece that is higher than the copper bond. The uniform movement of the heat source makes the heat conduction of each copper bond nearly uniform.

Therefore, in the second stage of meshing, a free tetrahedral mesh is still used. A very fine mesh is applied to the surface where the copper bond contacts the test piece, the upper surface of the test piece, and the heat transfer surface between the test piece and the fixture. The same boundary layer grid is applied, and the conventional mesh is applied to the copper bond; a coarse mesh was applied to the remainder. The meshing is shown in Figure 13.

### C. DERIVATION OF THE INLET VELOCITY RANGE

According to the design plan, the cross-sectional area of a single copper bond flow channel is $S = 12.53\ \text{mm}^2$, and a

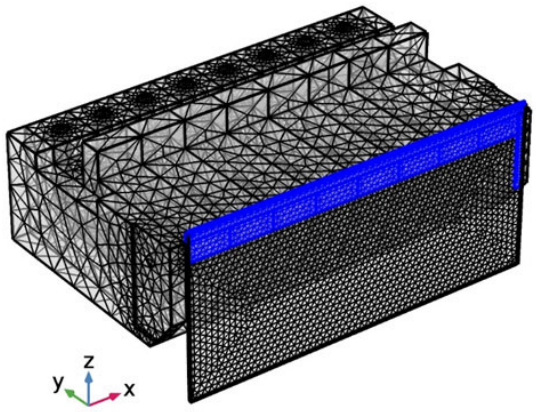


**FIGURE 13.** The second stage grid generation.

smaller cross-sectional area can produce a larger flow rate and Reynolds coefficient at a small flow rate. According to the principles of fluid mechanics, when the fluid traverses the heat exchange tube, the tail vortex will alternately fall off when the Reynolds coefficient reaches a certain level, which results in periodic lift and drag, and the Karman vortex excitation at the fluid inlet is defined as $fv$. In addition, a larger flow rate will also produce larger turbulent flow energy, causing the fluid to turbulently chatter, and its frequency is defined as ft. When the ratio of the natural frequency $fn$ to the heat exchange tube is greater than 0.5, the pipeline will produce copper bond resonance. Because the copper bond and the fixture are rigidly connected and there is an assembly gap between the copper bonds, resonance will adversely affect the trajectory of the welding gun and the shape of the molten pool during the welding process. Therefore, to establish a condition that ensures the turbulent heat transfer, the inlet flow rate of the pipeline must be limited.

In the new scheme, the flow path is inside the copper bond, and the shape of the copper bond is not uniform; thus, it is not suitable to use the natural frequency calculation method for the heat exchange tube with a clear wall thickness in GB/T151. Since each copper bond has the same size and flow channel size and is placed side by side, the natural frequency and vibration mode of each copper bond are taken to be the same. According to the Macdaff-Felga method and the derivation method recommended by RGP-RCB-4.562 in the 6th edition of TEMA, the calculation expression of the natural frequency of a single copper bond is the following:

$$f_n = \frac{154.8 C_n}{l^2} \sqrt{\frac{EJ}{mg}} \tag{7}$$

where $f_n$ is the natural frequency of the pipe with the same diameter; $C_n$ is the frequency constant, the subscript $n$ is the order of the vibration mode; $J$ is the moment of inertia of the cross-section, and the expression is $J = \frac{\pi d^4}{64}$; $d$ is the pipe diameter; and $g$ is the acceleration of gravity.

The calculation expression for the Carmen vortex excitation frequency is

$$f_v = St\frac{V}{d_0} \tag{8}$$

where $V$ is the inlet flow rate; $d_0$ is 5 mm; $S_t$ is the Stroha number, which is dimensionless; the inner flow path of the copper bond can be considered to be close to a square arrangement; and $S_t$ can be found in GB/T151 according to the pitch diameter ratio.

According to the side-by-side arrangement of the copper bonds and the pipeline direction inside the copper bonds, half of the fixture can be regarded as an overall heat exchanger. Then, the calculation formula for the turbulent buffeting frequency is

$$f_t = \frac{Vd_0}{lT}[3.05(1-\frac{d_0}{LT})^2 + 0.28] \tag{9}$$

where $l$ is the center distance of the inner runner of the adjacent copper bond, and $T$ is the upper and lower center distance of the inner runner of the single copper bond.

The calculated inlet flow velocity is $V \leq 6.7$ m/s, according to the flow velocity relationship, and the corresponding flow $Q$ of a single copper bond is obtained as $Q \leq 5$ L/min. Considering the structural difference between the actual structure of the copper bond and the heat exchange tube, the flow rate range of 2∼5 L/min is the optimal flow rate range of the flexible flow channel.

### D. MODEL EQUATION AND TRANSFORMATION

#### 1) TURBULENT HEAT TRANSFER EQUATION AND PARAMETER CALCULATIONS

Considering the *Re* value and the calculation time of the flow characteristics of water cooling in the smooth tube passage, the *k-ε* model is used to simulate the coupled field. The turbulent viscosity equation is shown in equation 10, where $C\mu$ is the model constant, and the value is 0.09.

$$\mu_T = \rho C_\mu \frac{k^2}{\varepsilon} \tag{10}$$

The transport equation with $k$ and $\varepsilon$ as unknowns is as follows:

$$\rho\frac{\partial k}{\partial t} + \rho\mathbf{u}\cdot\nabla k = \nabla\cdot\left(\left(\mu+\frac{\mu_T}{\sigma_k}\right)\nabla k\right) + G_k - \rho\varepsilon \tag{11}$$

$$\rho\frac{\partial \varepsilon}{\partial t} + \rho\mathbf{u}\cdot\nabla\varepsilon = \nabla\cdot\left(\left(\mu+\frac{\mu_T}{\sigma_\varepsilon}\right)\nabla\varepsilon\right) + C_{\varepsilon 1}\frac{\varepsilon}{k}P_k - C_{\varepsilon 2}\rho\frac{\varepsilon^2}{k} \tag{12}$$

where $G_k$ is the turbulent kinetic energy generation term:

$$G_k = \mu_T\left(\nabla\mathbf{u}:\left(\nabla\mathbf{u}+(\nabla\mathbf{u})^T\right) - \frac{2}{3}(\nabla\cdot\mathbf{u})^2\right) - \frac{2}{3}\rho k\nabla\cdot\mathbf{u} \tag{13}$$

The relationship between turbulent kinetic energy and the dissipation rate of turbulent energy is expressed as follows:

$$\varepsilon = 0.09\rho\frac{k^2}{\mu}\left(\frac{\mu_t}{\mu}\right)^{-1} \tag{14}$$

where $\mu_t/\mu$ represents the turbulent viscosity ratio, which is proportional to the Reynolds number.

Since the fluid flows along the x-axis, the expansion of equations 5∼8 are shown in equations 15∼17:

$$\frac{\partial(\rho k)}{\partial t} + \frac{\partial(\rho k u_i)}{\partial x_i} = \frac{\partial}{\partial x_j}\left[\left(\mu+\frac{\mu_t}{\sigma_k}\right)\frac{\partial k}{\partial x_j}\right] + G_k - \rho\varepsilon \tag{15}$$

$$\frac{\partial(\rho\varepsilon)}{\partial t} + \frac{\partial(\rho\varepsilon u_i)}{\partial x_i} = \frac{\partial}{\partial x_j}\left[\left(\mu+\frac{\mu_t}{\sigma_\varepsilon}\right)\frac{\partial\varepsilon}{\partial x_j}\right] + C_{1\varepsilon}\frac{\varepsilon}{k}G_k - C_{2\varepsilon}\rho\frac{\varepsilon^2}{k} \tag{16}$$

where $C_{1\varepsilon}$ and $C_{2\varepsilon}$ are empirical constants, $G_k$ is the generation term of turbulent kinetic energy, and its expansion formula is

$$G_k = \mu_t\left\{2\left[\left(\frac{\partial u}{\partial x}\right)^2 + \left(\frac{\partial v}{\partial y}\right)^2 + \left(\frac{\partial w}{\partial z}\right)^2\right] + \left(\frac{\partial u}{\partial y}+\frac{\partial v}{\partial x}\right)^2 + \left(\frac{\partial u}{\partial z}+\frac{\partial w}{\partial x}\right)^2 + \left(\frac{\partial v}{\partial z}+\frac{\partial w}{\partial y}\right)^2\right\} \tag{17}$$

The relevant model parameters set in this study are the following: $C_{1\varepsilon} = 1.44$, $C_{2\varepsilon} = 1.92$, $\sigma_k = 1.0$, and $\sigma_\varepsilon = 1.3$. The corresponding expression of the turbulence intensity $I$ is

$$I = \frac{u'}{\overline{u}} = 0.16\,(Re)^{-1/8} \tag{18}$$

#### 2) DERIVATION OF THE TEMPERATURE SOLUTION EQUATION OF THE COUPLED HEAT TRANSFER SECTION

In the repair process, the energy is transmitted from the blade to the fixture; part of the fluid in the runner is heated, and the heat transfer position of the fluid in the flow path changes with the movement of the heat source. The heat transfer of the coupling section is a nonisothermal flow problem, and the basic equation of the nonisothermal flow coupling heat transfer is shown in equation 19, where $\mathbf{F}$ is the flow force vector, $\mathbf{u}$ is the velocity vector, and $\mu$ is the dynamic viscosity.

$$\frac{\partial\rho}{\partial t} + \nabla\cdot(\rho\mathbf{u}) = 0$$

$$\rho\frac{\partial\mathbf{u}}{\partial t} + \rho\mathbf{u}\cdot\nabla\mathbf{u} = -\nabla p + \nabla\cdot\left(\mu\left(\nabla\mathbf{u}+(\nabla\mathbf{u})^T\right) - \frac{2}{3}\mu(\nabla\cdot\mathbf{u})\mathbf{I}\right) + \mathbf{F} \tag{19}$$

Because the turbulent energy transfer is a more complex form of energy transfer, based on the theory of fluid heat transfer, the nonisothermal flow calculation in this study uses the Favre average method to derive the equation. Let the

average value of Favre of the variable $T$ be expressed as $\tilde{T}$, which is defined as

$$\tilde{T} = \frac{\overline{\rho T}}{\bar{\rho}} \tag{20}$$

According to the definition of the Reynolds average, this formula can be divided as follows:

$$T = \tilde{T} + T'' \tag{21}$$

Therefore, the total internal energy equation can be expressed as

$$\begin{aligned}
&\frac{\partial}{\partial t}\left(\bar{\rho}\left(\tilde{e}+\frac{\tilde{u}_i\tilde{u}_i}{2}\right)+\frac{\overline{\rho u_i'' u_i''}}{2}\right)\\
&\quad+\frac{\partial}{\partial x_j}\left(\bar{\rho}\tilde{u}_j\left(\tilde{h}+\frac{\tilde{u}_i\tilde{u}_i}{2}\right)+\tilde{u}_j\frac{\overline{\rho u_i'' u_i''}}{2}\right)\\
&=\frac{\partial}{\partial x_j}\left(-q_j-\overline{\rho u_j'' h''}+\overline{\tau_{ij}u_i''}-\frac{\overline{\rho u_j'' u_i'' u_i''}}{2}\right)\\
&\quad+\frac{\partial}{\partial x_j}\left(\tilde{u}_i\left(\bar{\tau}_{ij}-\overline{\rho u_i'' u_j''}\right)\right)
\end{aligned} \tag{22}$$

where $q_j = -\lambda\frac{\partial T}{\partial x_j}$, $h$ is the enthalpy, $q_j$ is the expression of the vector heat flux, and $\lambda$ is the thermal conductivity.

The expression of the viscous stress tensor is

$$\tau_{ij} = 2\mu S_{ij} - \frac{2}{3}\mu\frac{\partial u_k}{\partial x_k}\delta_{ij} \tag{23}$$

Because the medium in the flow channel of the fixture is water, it can be considered an incompressible fluid. The stress tensor is modeled by the Boussinesq approximation:

$$-\overline{\rho u_i'' u_j''} = \bar{\rho}\tau_{ij}^T = 2\mu_T\left(\tilde{S}_{ij}-\frac{1}{3}\frac{\partial\tilde{u}_k}{\partial x_k}\delta_{ij}\right)-\frac{2}{3}\bar{\rho}k\delta_{ij} \tag{24}$$

where $k$ is the turbulent kinetic energy, which is expressed as

$$\bar{\rho}k = \frac{1}{2}\overline{\rho u_i'' u_i''} \tag{25}$$

In equation 22, the turbulent heat transfer relation model of $u_j''$ and $h''$ can be considered to be similar to laminar heat flux, which can be expressed as

$$\overline{\rho u_j'' h''} = q_j^T = -\lambda_T\frac{\partial\tilde{T}}{\partial x_j} = -\frac{\mu_T C_p}{Pr_T}\frac{\partial\tilde{T}}{\partial x_j} \tag{26}$$

where $\bar{\tau}_{ij}\bar{U}_i''$ and $\overline{\rho u_j'' u_i'' u_i''/2}$ can be simulated by the extension of the terms for molecular diffusion and turbulent transport in the incompressible $k$ equation:

$$\overline{\tau_{ij}u_i''}-\frac{\overline{\rho u_j'' u_i'' u_i''}}{2} = \left(\mu+\frac{\mu_T}{\sigma_k}\right)\frac{\partial k}{\partial x_j} \tag{27}$$

Substituting equations 23∼27 into equation 16, the equation is as follows:

$$\begin{aligned}
&\frac{\partial}{\partial t}\left(\bar{\rho}\left(e+\frac{\tilde{u}_i\tilde{u}_i}{2}+k\right)\right)+\frac{\partial}{\partial x_j}\left(\bar{\rho}\tilde{u}_j\left(\tilde{h}+\frac{\tilde{u}_i\tilde{u}_i}{2}+k\right)\right)\\
&=\frac{\partial}{\partial x_j}\left(-q_j-q_j^T+\left(\mu+\frac{\mu_T}{\sigma_k}\right)\frac{\partial k}{\partial x_j}\right)\\
&\quad+\frac{\partial}{\partial x_j}\left(\tilde{u}_i\left(\overline{\tau_{ij}}+\bar{\rho}\tau_{ij}^T\right)\right)
\end{aligned} \tag{28}$$

The Favre average method is applied to the momentum equation by equation 24, and the following results are obtained:

$$\frac{\partial}{\partial t}\left(\bar{\rho}\tilde{u}_i\right)+\frac{\partial}{\partial x_j}\left(\bar{\rho}\tilde{u}_j\tilde{u}_i\right) = -\frac{\partial p}{\partial x_j}+\frac{\partial}{\partial x_j}\left(\bar{\tau}_{ij}+\bar{\rho}\tau_{ij}^T\right) \tag{29}$$

Taking the inner product between $\tilde{u}_i$ and equation 29, the analytical kinetic energy equation can be obtained from equation 28 as follows:

$$\begin{aligned}
&\frac{\partial}{\partial t}(\bar{\rho}(e+k))+\frac{\partial}{\partial x_j}\left(\bar{\rho}\tilde{u}_j(\tilde{e}+k)\right) = -\bar{p}\frac{\partial\tilde{u}_j}{\partial x_j}\\
&\quad+\frac{\partial}{\partial x_j}\left(-q_j-q^T j+\left(\mu+\frac{\mu_T}{\sigma_k}\right)\frac{\partial k}{\partial x_j}\right)\\
&\quad+\frac{\partial}{\partial x_j}\left(\tilde{u}_i\left(\tau_{ij}+\bar{\rho}\tau_{ij}\right)\right)
\end{aligned} \tag{30}$$

where $\tilde{h} = \tilde{e}+\bar{p}/\bar{\rho}$. For the incompressible fluid in the fixture, the contribution of $k$ can be ignored, and the equation can be transformed into the following:

$$\begin{aligned}
&\frac{\partial}{\partial t}(\bar{\rho}e)+\frac{\partial}{\partial x_j}\left(\bar{\rho}\tilde{u}_j e\right)\\
&\quad=-\bar{p}\frac{\partial\tilde{u}_j}{\partial x_j}+\frac{\partial}{\partial x_j}\left(-q_j-q_j^T\right)+\frac{\partial}{\partial x_j}\left(\tilde{u}_i\left(\bar{\tau}_{ij}+\bar{\rho}\tau_{ij}^T\right)\right)
\end{aligned} \tag{31}$$

Let $\bar{\tau}_{ij} = \tilde{\tau}_{ij}+\overline{\tau_{ij}''}$. Because $\tilde{\tau}_{ij} \gg \overline{\tau_{ij}''}$, for most engineering applications $\overline{\tau_{ij}} \approx \tilde{\tau}_{ij}$. Therefore,

$$\begin{aligned}
&\frac{\partial}{\partial t}(\bar{\rho}\tilde{e})+\frac{\partial}{\partial x_j}\left(\bar{\rho}\tilde{u}_j\tilde{e}\right)\\
&\quad=-\bar{p}\frac{\partial\tilde{u}_j}{\partial x_j}+\frac{\partial}{\partial x_j}\left((\lambda+\lambda_T)\frac{\partial\tilde{T}}{\partial x_j}\right)+\frac{\partial}{\partial x_j}\left(\tilde{u}_i\tilde{\tau}_{ij}^{\mathrm{Tot}}\right)
\end{aligned} \tag{32}$$

where

$$\tilde{\tau}_{ij}^{\mathrm{Tot}} = (\mu+\mu_T)\left(2\tilde{S}_{ij}-\frac{2}{3}\frac{\partial\tilde{u}_k}{\partial x_k}\delta_{ij}\right) \tag{33}$$

The fluid in the flow passage is water, which can be considered as $\bar{\rho} = \rho$, and the temperature equation on the conjugate heat transfer interface of the nonisothermal flow in turbulence model is

$$\begin{aligned}
&\rho C_p\left(\frac{\partial\tilde{T}}{\partial t}+\tilde{u}_j\frac{\partial\tilde{T}}{\partial x_j}\right)\\
&=\frac{\partial}{\partial x_j}\left((\lambda+\lambda_T)\frac{\partial\tilde{T}}{\partial x_j}\right)+\tilde{\tau}_{ij}\tilde{S}_{ij}-\frac{\tilde{T}}{\rho}\frac{\partial\rho}{\partial\tilde{T}}\bigg|_{\bar{p}}\left(\frac{\partial\bar{p}}{\partial t}+\tilde{u}_j\frac{\partial p}{\partial x_j}\right)
\end{aligned} \tag{34}$$

### *E. NUMERICAL ANALYSIS OF THE PRE-COOLING EFFECT*

According to the fluid equation and initial value conditions, we set the initial temperature of the copper bond to 70 °C; the test piece temperature to 20 °C; the fluid inflow temperature to 10 °C; and the flow rate to 5 L/min. We establish a coupled heat and heat transfer temperature model. Using the Algebraic Multigrid Solver to solve the transient coupled heat transfer process, we set the relative tolerance for the physics control, while the time step is a backward differential, and we use free steps long.

According to the calculation results, the temperature distribution inside the copper bond under the initial state of heat transfer at $t = 0.1$ s is shown in Figure 14. In the figure, the legend on the left represents the temperature isosurface, and the legend on the right represents the surface temperature of the copper bond in °C. The results show that at the beginning of the heat transfer, the overall temperature is higher because the effective heat conduction has not been established inside the copper bond. However, at the portion where the front end of the copper bond is in contact with the test piece, due to the solid heat transfer with the test piece, the temperature is relatively low, which results in a weak isotherm distribution in the local area.

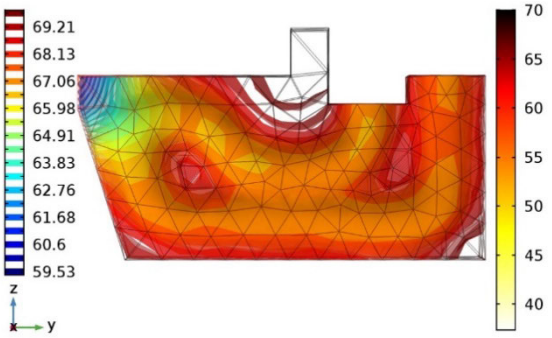


**FIGURE 14.** Temperature distribution inside the copper bond at the beginning of heat transfer (°C).

The heat transfer starts, and the temperature distribution inside the copper bond at $t = 2$ s is shown in Figure 15. The calculation results show that when the fluid starts to be turbulent, the copper bond temperature decreases rapidly, and the lowest temperature of the fluid decreases to 24.67 °C. In addition, the isothermal surface is densely spread outward from the fluid, and the copper bond as a whole drops by approximately 35 °C. A weak isotherm distribution of the copper bond corners disappears, and it becomes an isothermal surface that diverges from the position closest to the flow path.

The temperature distribution inside the copper bond at $t = 6$ s is shown in Figure 16. The overall temperature of the copper bond is reduced by approximately 58 °C, the temperature of the contact surface is reduced to 12.26 °C, and the distribution of the isothermal surface is denser. At this time, a better cooling cycle has been formed and is about to reach a steady state.


**FIGURE 15.** Temperature distribution in the copper bond at 2 s (°C).

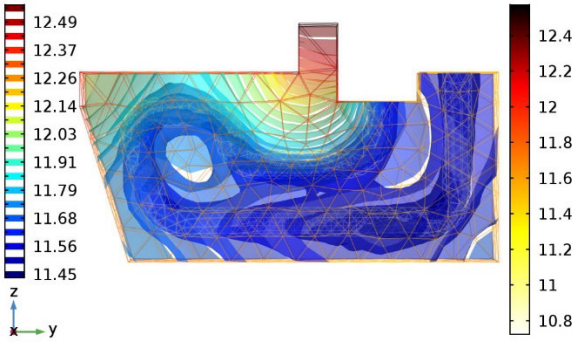


**FIGURE 16.** Temperature distribution in the copper bond at 6 s (°C).

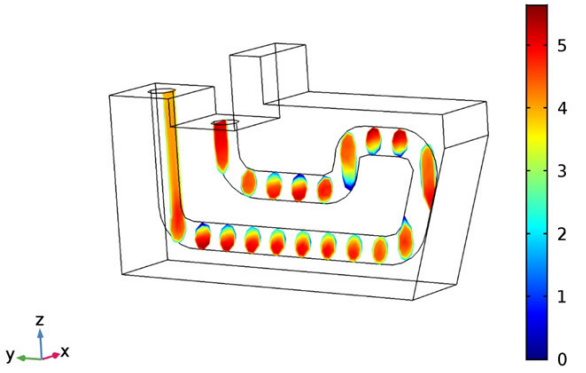


**FIGURE 17.** Flow velocity at different cross-sections of the flow path at t=6 s (m/s).

The flow velocity at different cross-sections of the flow path at $t = 6$ s is shown in Figure 17. The flow path turning closest to the contact surface of the copper bond and the test piece is defined as the third turning. The calculation results show that there is no obvious attenuation of the flow velocity at the third turn, and there is a constant velocity surface with a flow velocity of approximately 5 m/s, which can quickly remove the heat from the contact surface. After the third turn of the fluid, a short-term acceleration of approximately 5.5 m/s is formed on the wall surface close to the upper surface of the copper bond, which will also help the rapid heat dissipation of the upper surface of the copper bond.

Taking the contact surface of the copper bond and the test piece as the research object, we keep the initial value consistent with the boundary conditions. The inlet flow rates

are set to 2 L/min, 3 L/min, and 5 L/min. Through the calculation, the temperature change value of the contact surface is obtained within 20 s, and the change of the contact surface cooling temperature with time under different cooling conditions, as shown in Figure 18. The graph shows that the cooling rate of the new method is significantly better than fixture base cooling and natural cooling. The flow rates of 2 L/min, 3 L/min and 5 L/min can cool the copper bond from 70 °C to nearly 10 °C within 8 s. As shown by the temperature change curve, before 6 s the temperature decreases faster with an increase in the flow rate; the temperature of 5 L/min decreases fastest, and the temperature decreases relatively slowly at 2 L/min. However, after approximately 6 s, as the temperature difference decreases, the rate of the temperature decrease at all three flow rates tends to be gentle. At approximately 10 s, the contact surface and the fluid temperature are basically the same, and the heat conduction of the fixture reaches a stable state.

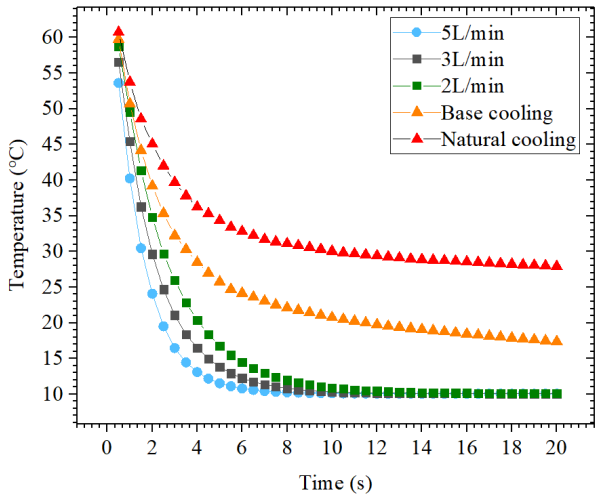


**FIGURE 18.** Cooling effect of the contact surface under different cooling conditions (m/s).

### *F. NUMERICAL ANALYSIS OF HEAT TRANSFER IN BLADE REPAIR*

#### 1) THE HEAT TRANSFER ISOSURFACE AND TEMPERATURE DISTRIBUTION OF NEW COPPER BOND

Taking the model state where the fixture reaches steady-state heat conduction in the first stage as the initial condition, the flow velocity at the inlet of the flow path is set to 2 L/min, 3 L/min, and 5 L/min. To compare the cooling effects, the height of the upper surface of the test piece is the same as the height as that of the base cooling method, and the remaining boundary conditions are set to the same boundary conditions as the model in the base cooling method. Then, the numerical analysis of the heat flow coupled heat transfer process after the test piece is loaded with a heat source is performed. Since the middle part of the fixture is the relatively stable part of the heat transfer, we select the fourth copper bond near the middle position as the analysis object, and we

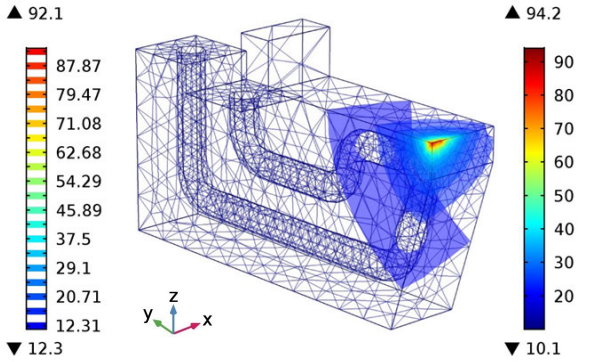


**FIGURE 19.** Heat transfer isosurface and temperature distribution of the copper bond (t=18.3 s, °C).

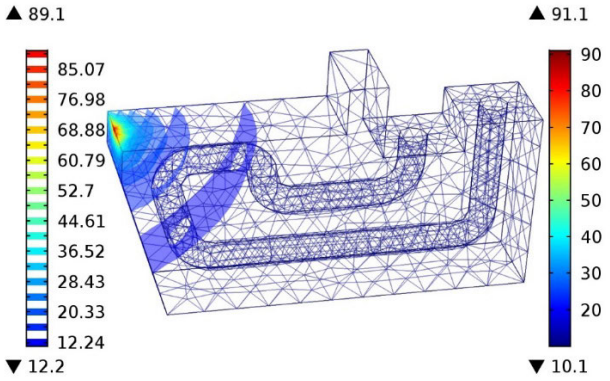


**FIGURE 20.** Heat transfer isosurface and temperature distribution of the copper bond (t=21.3 s, °C).

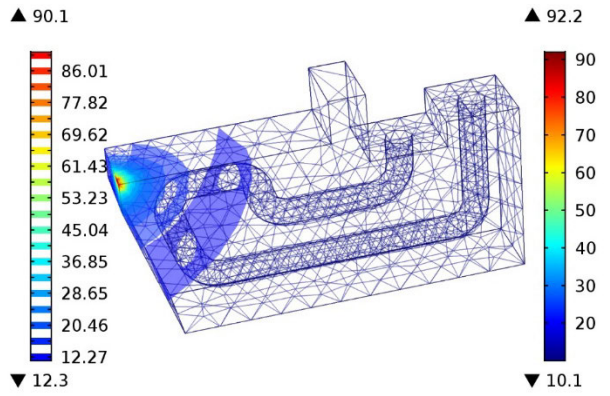


**FIGURE 21.** Heat transfer isosurface and temperature distribution of the copper bond (t=24.3 s, °C).

set the flow rate to 3 L/min. Then, according to the moving speed of the heat source and the coordinate position of the fourth copper bond, the time for the heat source to move to the end of the fourth copper bond is calculated to be 18.3 s, the time for the heat source to move to the middle of the fourth copper bond is 21.3 s, and the time for the heat source to move out of the fourth copper bond is 24.4 s. The simulation shows that the temperature and isosurface distribution of the copper bonds at three time points are shown in Figures 19 to 21.

Considering the time period from 18.3 s to 24.4 s, in other words, the time period when the heat source moves in the

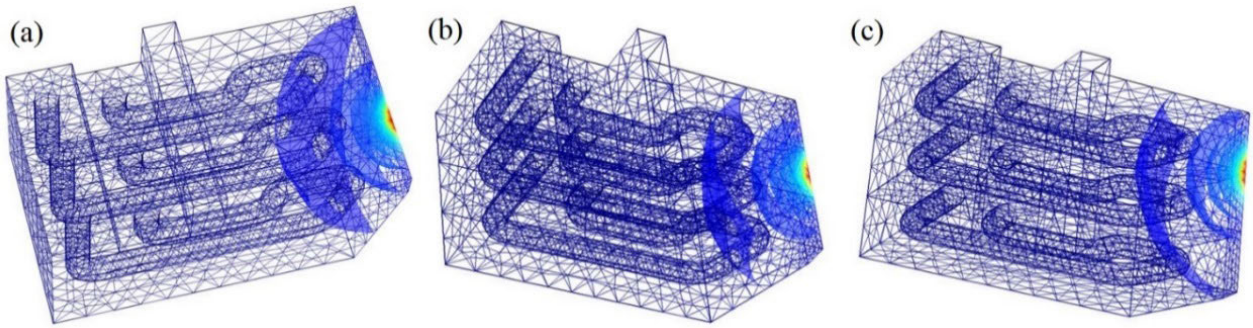


**FIGURE 22.** (a)The position of the isothermal surface in the adjacent copper bond at 18.3 s. (b) The position of the isothermal surface in the adjacent copper bond at 21.3 s. (c) The position of the isothermal surface in the adjacent copper bond at 24.3 s.

position area of the upper surface corresponding to the fourth copper bond, it can be seen from the heat transfer isosurface of the copper bond that the fluid participates continuously in heat transfer and maintains more stable heat conduction efficiency. Since most of the copper bonds have been pre-cooled to 10 °C by the flow path, heat is quickly diffused and transferred from the contact point. At 18.3 s, the highest temperature of the copper bond is 94.2 °C.

When the heat source moves to the upper surface of the test piece, which corresponds to the center of the copper bond, the heat source is closest to the flow path, and the maximum temperature of the copper bond decreases. As the welding continues, the heat source gradually leaves above the copper bond. At 24.3 s, the heat source is above the other corner of the copper bond and is about to leave the $x$-axis coordinate interval of the copper bond and enter the x-axis coordinate interval of the next copper bond. It can be seen from Figures 19 to 21 that when the maximum temperature is near the corner of the copper bond, the equivalent value is significantly inclined toward the direction of the flow path. As the heat source moves, the angle of inclination gradually decreases, and the isothermal surface presents a symmetrical distribution when it reaches the middle position, and then, it tilts again. On the copper bond body, the temperature after the last isothermal surface always stays in the range 10∼12 °C. The flexible flow path cooling method can only can take away the energy transferred by the heat source but can also continuously maintain most of the copper bonds at a lower temperature, which is conducive to rapid heat conduction inside the copper bond.

Next, we add the adjacent third copper bond and fifth copper bond, and we set the same isothermal surface interval and the number of layers. The simulation results are shown in Figure 22. When the heat source passes over the middle copper bond, the flow paths in the adjacent copper bonds also participate in heat exchange. The positions of the isothermal surfaces in Figure 22(a) and 22(c) are basically symmetrical. It can be inferred that each time the heat source sweeps a copper bond, the fluids in the two adjacent copper bonds participate in heat exchange. In addition, the entire fixture is in a near-steady heat transfer state during the welding process.

### 2) FLUID HEAT TRANSFER BOUNDARY STATE AND TEMPERATURE DISTRIBUTION

In the welding process, the heat transfer of the fluid in a flexible multiflow path can be considered to have two boundary states: one boundary state is the moment when the heat source is located directly above the cross-section of the copper bond, and the other boundary state is the moment when the heat source is located at the corner of the copper bond. Taking the fourth copper bond as an example, the temperature distribution of the fluid in the two boundary states is shown in Figures 23 and 24.

When the heat source moves to the test piece upper surface directly above the cross-section of the copper bond, the maximum temperature of the fluid in the corresponding copper bond reaches 14.6 °C. At this time, the heat spreads mostly in the $y$-$z$ cross-section. There are 3 participating heat exchange fluids, of which the intermediate fluid is the main heat exchange fluid, and the fluid in the two adjacent copper bonds facilitates the heat exchange.

When the heat source moves above to the test piece upper surface directly at the corner point of the copper bond, the cross-section of the heat source is exactly the contact surface of the two copper bonds, and the distance from the flow channels on the two sides is equal. At this time, the heat diffuses in the direction of the two flow paths and expands the isothermal surface into the fluid of the second copper bond on both sides. The maximum temperature of the fluid on both sides is approximately 14.08 °C, and 4 fluids are participating in the heat exchange.

The change in the maximum temperature of the fluid over time at different flow rates is shown in Figure 25. The results show that the maximum temperature fluctuation trend of the fluid at three flow rates is basically the same. At the beginning and the end of the welding, the copper bonds at both ends of the fixture are in contact with air, and the heat conduction is slow; as a result, the temperature of the fluid near the two ends is high. In a welding process of 5∼45 s, with the movement of the heat source, the fluid temperature fluctuation is relatively stable. When the heat source moves directly above the cross-section of the copper bond, the fluid temperature is the highest; when the heat source is located between the two

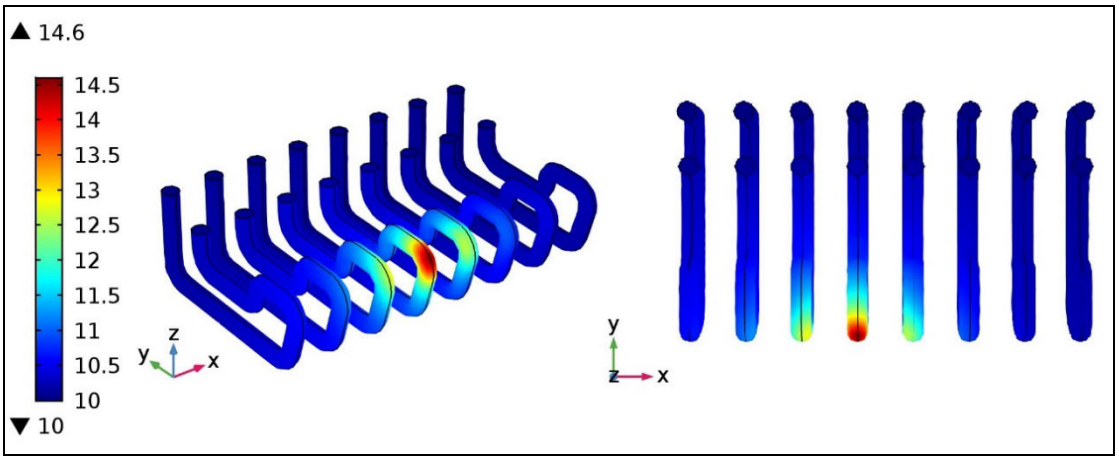


**FIGURE 23.** Temperature distribution of the fluid when the heat source is directly above the copper bond.

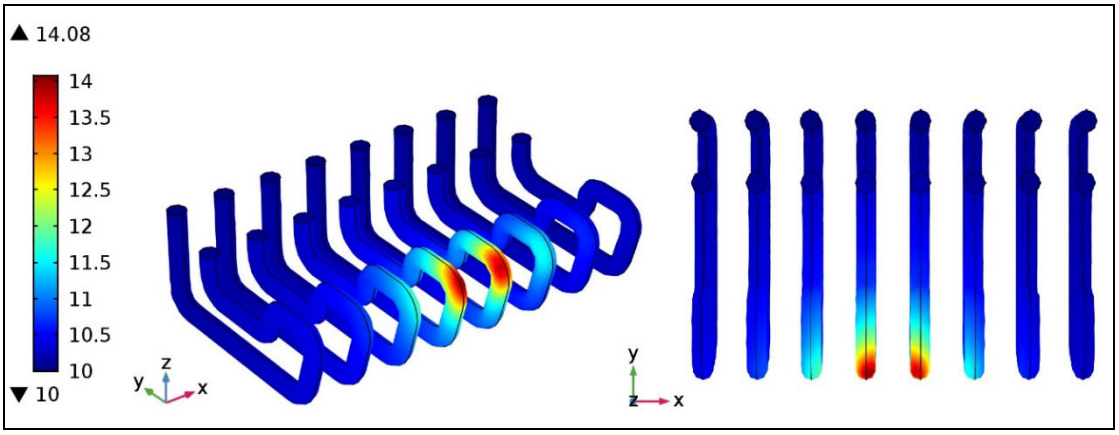


**FIGURE 24.** Temperature distribution of the fluid when the heat source is above the copper bond corner.

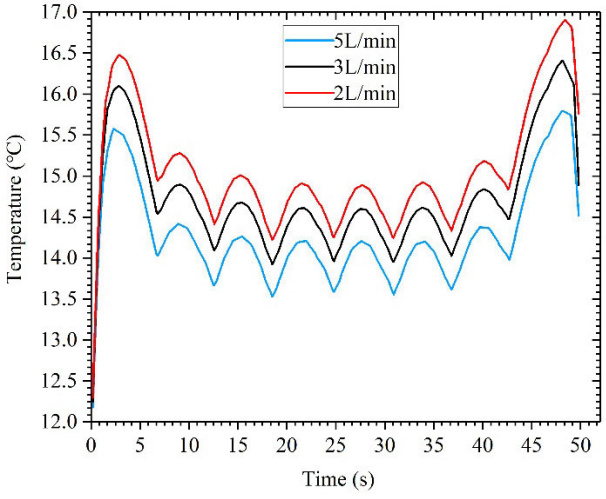


**FIGURE 25.** The change in the maximum temperature of the fluid with time at different flow rates.

copper bonds, the fluid temperature is the lowest. Therefore, the curve shows a regular wave state. From the perspective of the temperature fluctuation of the fluid, the heat conduction of the whole fixture is in a relatively stable regular state, which will provide stable and fast cooling effect in repair.

### 3) COOLING EFFECT OF A TYPICAL FIXTURE CROSS-SECTION

Two typical cross-sections on the fixture are analyzed. First, the middle section of the fourth copper bond is taken as typical section 1, as shown in Figure 26. This cross-section is exactly the cross-section of the fourth copper bond and the internal fluid, and it is close to the middle of the fixture. The heat transfer is relatively stable, and it is less affected by the copper bonds on both sides.

When the heat source moves to the test piece upper surface directly above the cross-sectional position, 4 s before and after this time, 17.4∼25.4 s, is taken as the cooling time reference time interval. The change in the maximum temperature of cross-section 1 with time under different cooling conditions is shown in Figure 27. The red curve is the temperature change of cross-section 1 in the fixture base cooling method (a result of the numerical analysis under the condition of 5.5 L/min). The other three colored curves are the maximum temperature change curves of cross-section 1 at

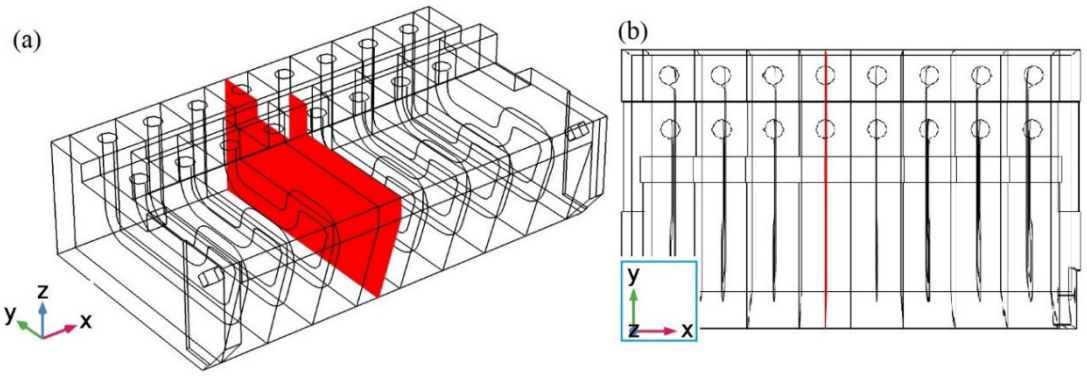


**FIGURE 26.** (a)Three-dimensional location sketch of section 1. (b) Top view of section 1 location.

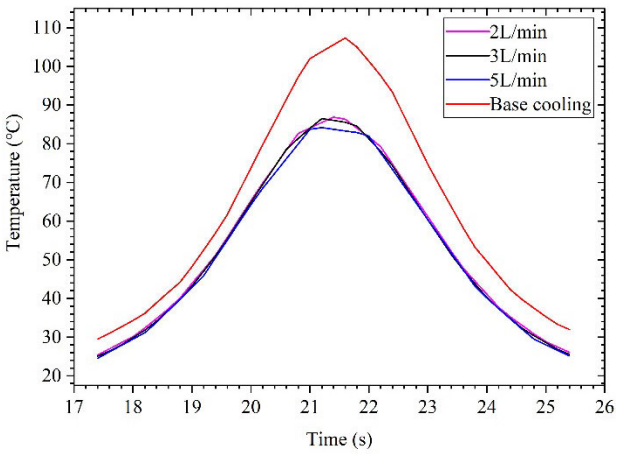


**FIGURE 27.** Maximum temperature change of section 1.

flow rates of 2 L/min, 3 L/min and 5 L/min with the flexible flow path cooling method.

The results of the curve analysis show that the maximum temperature of cross-section 1 with the flexible flow path cooling method is significantly lower than that determined with the base cooling method. According to the previous simulation results shown in of Figure 20, the maximum temperature of the cross-section appears at the corner of the contact surface between the copper bond and the test piece. According to Newton's cooling law, the temperature difference between the contact surface and the test piece has a direct impact on the heat dissipation gradient of the test piece. Under the three flow rate conditions of the flexible flow channel, the maximum temperature of the contact surface at the flow rate of 5 L/min is slightly lower than that of the other two flow rates, and the maximum temperatures of the contact surface at the flow rate of 3 L/min and 2 L/min are very similar.

We take the position of the contact surface of the fourth copper bond and the fifth copper bond as typical cross-section 2, which is shown in Figure 28. This cross-section is close to the center of the fixture and is located on the symmetry plane of the fourth and fifth flow paths. There is no fluid on cross-section 2, which is only the boundary state of the copper bond heat source. We still consider the 4 s before and after the heat source moves to the cross-sectional position, which is 20.4∼28.4 s, to be the cooling time reference time interval.

The change in the maximum temperature of the cross-section with time under different cooling conditions is shown in Figure 29. Although there is no fluid part on typical cross-section 2, because it is located between the two flow paths, according to the calculation results in Figure 23, there are still four flow paths that participate in heat transfer at the same time, and thus, the maximum temperature of cross-section 2 is still approximately 30 °C lower than the base cooling method. The typical cross-section 1 and the typical cross-section 2 can be regarded as sandwiching two specific microelements, $dx_1$ and $dx_2$. The curve of the two cross-sections is basically the same. It can be inferred that the fixture maintains a relatively stable temperature throughout the welding process, and each cross-section maintains stable heat transfer efficiency.

#### 4) TEMPERATURE DISTRIBUTION OF THE WELD CROSS-SECTION

To compare the cooling effect of the flexible flow path cooling method at different flow rates, based on the previous heat input study, we set the same additive manufacturing repair height (twice the additive height) of the test piece and take the same position of the weld cross-section. We remove the 2 s at the beginning and end of the welding, take a more stable time interval of 2∼48 s during the welding process, and set the sampling step to 0.1 s. The numerical values of the weld cross-section temperature at three cooling rates are fitted in the form of dot plots of different colors, and the average temperature (average value of the maximum temperature of the weld micro section) distribution of the weld cross-section under different flow rates is shown in Figure 30.

The results show that at three flow rates of the new method, the average temperature of the micro section of the weld cross-section is approximately 140∼160 °C lower than that of the current method (fixture base cooling). At the 5 L/min flow rate of the new cooling method, the cooling efficiency

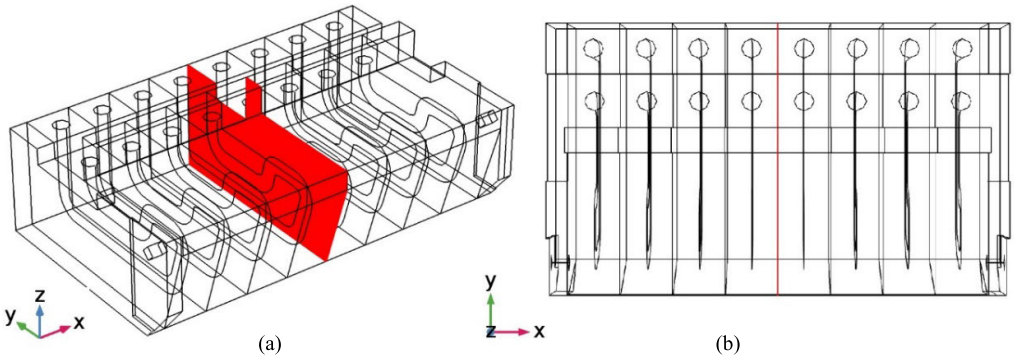


**FIGURE 28.** (a)Three-dimensional location sketch of section 2; (b) Top view of section 2 location.

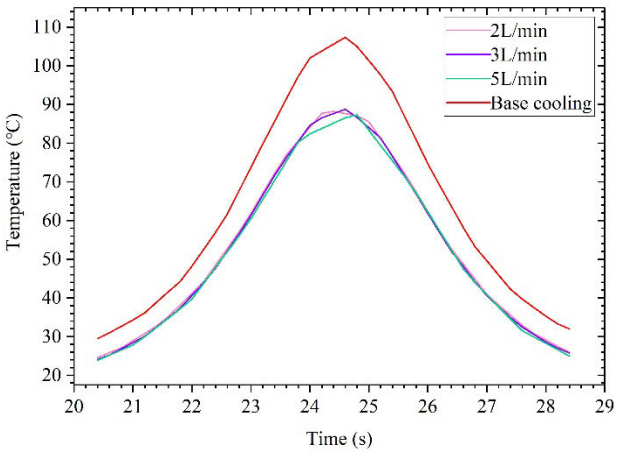


**FIGURE 29.** Maximum temperature change of section 1.

is highest, and the maximum temperature of the weld can be reduced to approximately 1224 °C. In terms of the weld temperature fluctuations, the temperature fluctuation range is the smallest at a flow rate of 3 L/min, and it is denser on the temperature line at approximately 1320 °C, followed by 2 L/min, and the largest at 5 L/min. In the case of a three-time additive repair or a larger height additive repair, it is necessary to comprehensively consider the cooling rate and the temperature fluctuation of the molten pool. In the case of a small amount of local additive repair, due to the small molten pool, the temperature fluctuations over a short time can be ignored, and thus, a flow rate of 5 L/min can be used to achieve rapid cooling. For additive manufacture repair with long welds, using a flow rate of less than 3 L/min is expected to achieve better melt pool morphology and welding quality.

### G. PRESSURE CALCULATION AT DIFFERENT FLOW RATES

The pressure distribution of the flow paths at different flow rates is shown in Figure 31. The distribution of the pressure contours of the flow paths at the three flow rates is basically the same. The isoline with a higher pressure is distributed at the entrance of the flow channel. At the position of the flow channel closest to the contact surface, the pressure is maintained at more than 70% of the inlet pressure, which can maintain the fluid in a large turbulent state. The position where the fluid pressure is small is the straight pipe closest to the outlet, where the fluid has already participated in the heat exchange and needs to flow out of the flow channel quickly; as a result, negative pressure is formed at the outlet. According to the calculation results of the maximum inlet pressure, the inlet pressure at a flow rate of 3 L/min is approximately twice the inlet pressure at a flow rate of 2 L/min, and the inlet pressure at a flow rate of 5 L/min is the largest, with a value of approximately 102 kPa, which increases 5-fold at a 2 L/min flow rate. According to the inlet pressure at different flow rates, a pressure regulator must be installed on the pipeline to make the flow rate reach the set value. In addition, when connecting and sealing the coolant pipeline, the design pressure of the pipeline should reach more than 1.5-fold the calculated value. The purpose is to meet the pressure requirements of the system.

## V. EXPERIMENTAL SETUP

According to the structural design of the flexible multiflow path fixture, the ideal processing and manufacturing scheme of the copper bond is precision casting or 3D printing. However, since the fixture is made of copper and the flow path is located inside the copper bond, it is difficult to cast, and there are still many difficulties in high-precision copper 3D printing technology, which must be further studied. For these reasons, the fixture experimental prototype uses the machining center to mill out the flow channel for half of the copper bond, and then, they are spliced and glued into a whole. The experimental prototype of the assembled flexible multiflow path fixture is shown in Figure 32.

Referring to the design scheme in Fig. 8 and Fig. 9, there are 8 movable copper bonds on both sides of the flexible fixture, and a flow path is designed inside the copper bond. The inlet and outlet of the flow path are connected with the buffer by flexible pipes. We initially used a small water pumps for each tube, the total number of pumps is 16. However, although this scheme can control the flow of each tube independently, the control and adjustment are complicated due to the large number of pumps. Therefore, we used two larger

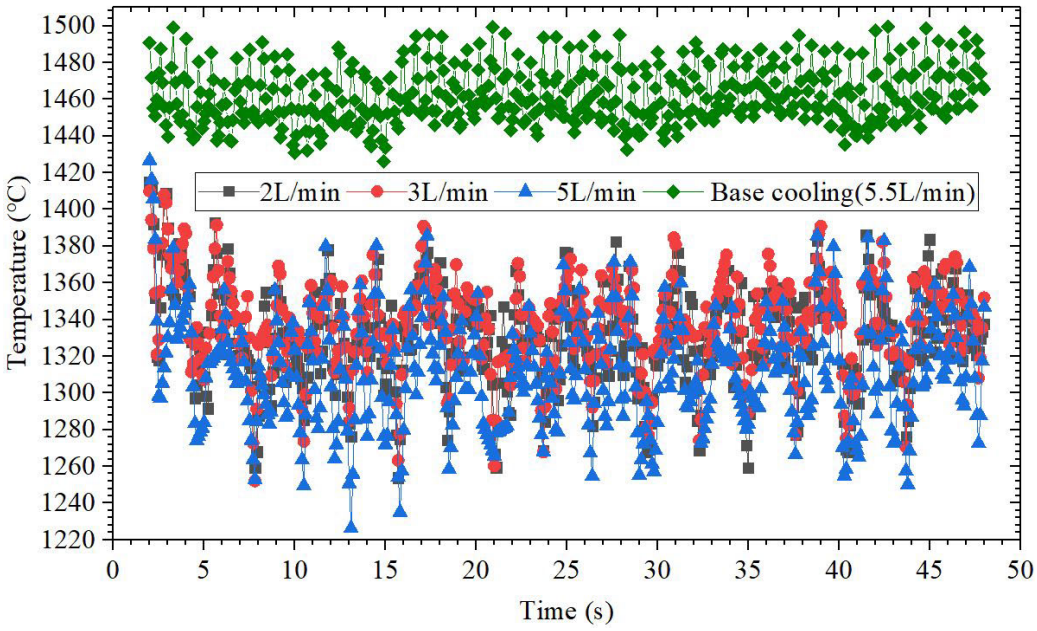


**FIGURE 30.** Comparison of the micro section average temperature distribution of the weld cross-section (new method vs current method).

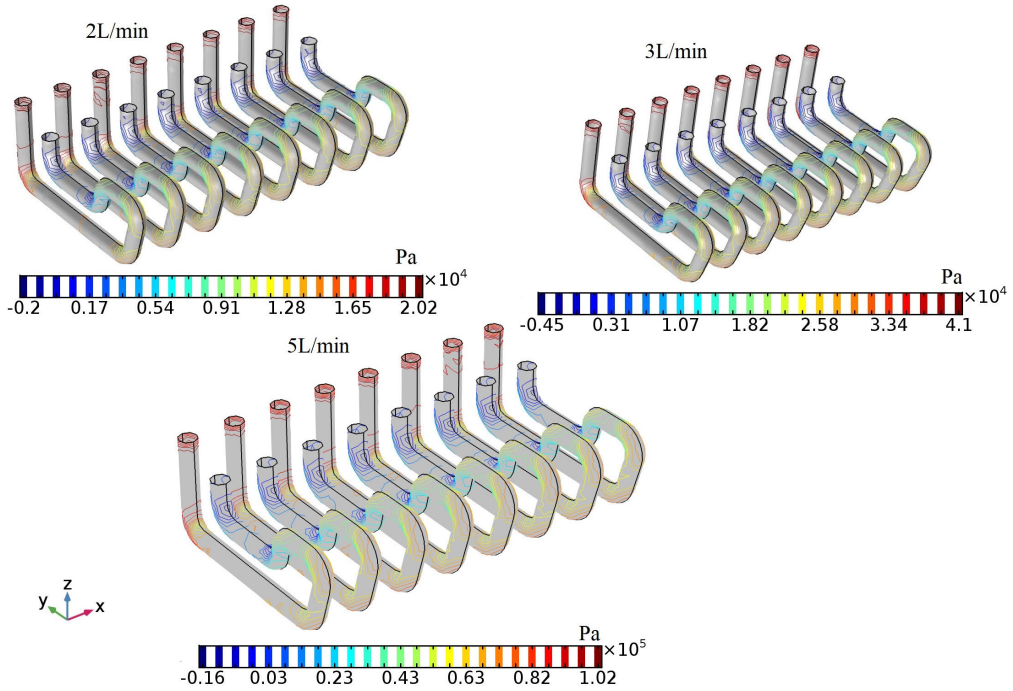


**FIGURE 31.** Pressure distribution of the flow passage at different flow rates (Pa).

pumps, through the total adjustment and buffer to balance the flow in each tube.

In order to compare the experimental results with the simulation results and verify the cooling effect, firstly, the pre-cooling experiment of the fixture prototype is carried out. Half of the fixture is heated to 150 °C in the heating box and then taken out quickly. When the temperature drops to 70 °C, the water cooling system is started and the flow rate in single flow path is adjusted to 3 L/min. The fourth to sixth copper bonds in the middle are selected as the research objects, and the average temperature of the three copper bonds is measured with time. The laboratory temperature was

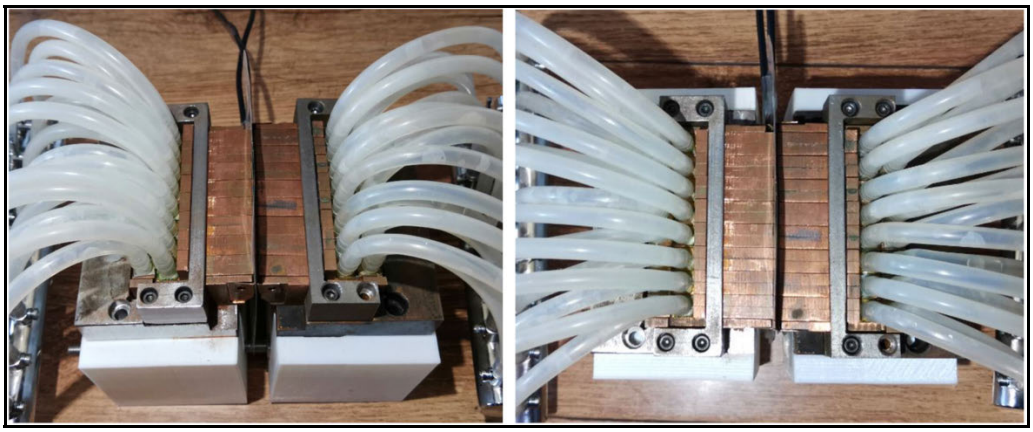

**FIGURE 32.** Flexible multiflow Path fixture prototype.

**TABLE 2.** Comparison between experiment and simulation (°C).

| 3 L/min \Time | 1s | 2s | 3s | 4s | 5s | 6s | 7s | 8s | 9s | 10s | 11s | 12s | 13s | 14s | 15s |
|---|---|---|---|---|---|---|---|---|---|---|---|---|---|---|---|
| Simulation | 45.4 | 29.6 | 21.1 | 16.5 | 13.8 | 12.3 | 11.4 | 10.8 | 10.5 | 10.3 | 10.2 | 10.2 | 10.1 | 10.1 | 10.1 |
| Experiment | 48.9 | 34.7 | 25.1 | 21.5 | 16.9 | 14.3 | 13.2 | 12.3 | 11.4 | 11.1 | 10.9 | 10.8 | 10.8 | 10.7 | 10.7 |

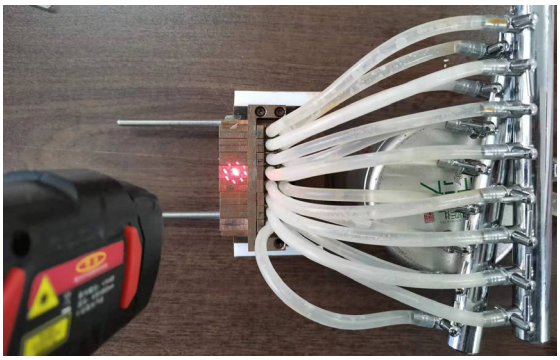

**FIGURE 33.** Precooling experiment of the fixture prototype.

20 °C, the cooling water temperature was 10 °C. The experimental results are shown in Table 2. Then, these results are compared with the simulation results of Figure 18, as shown in Figure 34.

The experimental temperature gradient and change rate are consistent with the trend of the simulation results, and the experimental temperature is slightly higher than the simulation. Considering the assembly error and the micro gap thermal resistance [31] between the copper bonds, the experimental results are in good agreement with the simulation results, and the expected effect on the pre cooling is achieved

Because the fixture is still in the prototype stage, it cannot be installed on the MPAW system for the overall welding test, so the experimental part of this paper is mainly to test the cooling effect. In the prototype experiment, an electric heating piece was used instead of the alloy test piece. After the electric heating piece was heated to 100 °C, the power was cut off. The heating piece area that corresponded to the copper key in the middle of the fixture was selected as the temperature measurement object. The infrared thermometer was used to detect the temperature change of the heating piece under different flow rates, and the measurement position was the contact surface between the heating piece and the copper bonds. The connection of the copper bond flow path is in parallel. To achieve the flow rate of 2 L/min and 3 L/min for a single copper bond, the flow rate of a single side circulating pump was adjusted to 16 L/min and 24 L/min, respectively. The experimental results are shown in Table 3 and Figure 35.

The results show that the new cooling method can achieve a good cooling effect. The flow rate of 0 L/min can be regarded as natural cooling; the cooling speed of the test area decreases after 5 s and becomes slower when the temperature drops

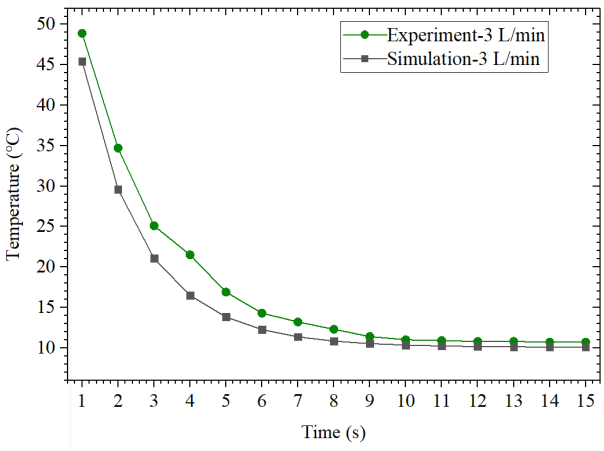


**FIGURE 34.** Comparison between experiment and simulation.

**TABLE 3.** Temperature change of the heating plate at different flow rates (°C).

| Flow rate\Time | 2s | 3s | 4s | 5s | 6s | 7s | 8s | 9s | 10s | 11s | 12s | 13s | 14s |
|---|---|---|---|---|---|---|---|---|---|---|---|---|---|
| 0 L/min | 94.3 | 78.8 | 62.7 | 55.8 | 51.1 | 47.5 | 43.4 | 41.9 | 39.8 | 37.7 | 35.3 | 33.9 | 32.2 |
| 2 L/min | 82.8 | 60.2 | 43.9 | 39.7 | 28.4 | 23.1 | 20.1 | 18.2 | 16.0 | 15.3 | 14.6 | 14.0 | 13.5 |
| 3 L/min | 82.5 | 59.1 | 43.3 | 39.3 | 28.2 | 22.5 | 19.2 | 17.1 | 15.7 | 14.7 | 13.9 | 13.3 | 12.8 |

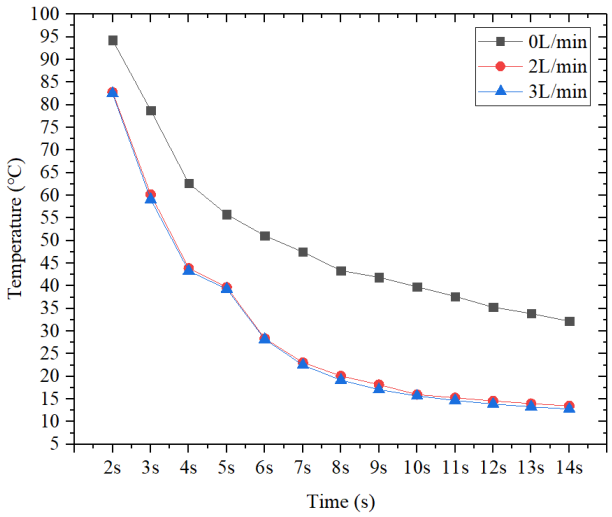


**FIGURE 35.** Temperature change of the test area at different flow rates.

below 40 °C. With the increase in the flow rate, the temperature of the test area continues to decrease, and it can drop to a temperature that is approximately equal to room temperature in 8 s. Afterward, the temperature continues to decrease, and it is expected to reach a temperature value close to that of the fluid in the end. In terms of the flow rate, the cooling effect of 3 L/min is slightly better than that of 2 L/min, but considering the detection error and machining accuracy in the flow path, the cooling effect of the two flow rates can be considered to be very similar. Therefore, 2 L/min with smaller pipeline pressure can be selected as the cooling parameter.

In addition, the water cycle test of 4∼8.5 L/min was conducted. When the flow rate of single path is greater than 5 L/min, the fixture has obvious resonance. It can be inferred that the resonance is mainly caused by turbulent energy and pipe resistance, which require further study. When the flow rate is approximately 8 L/min, the pipeline pressure reaches approximately 343.2 kPa, and leakage occurs at the external interface and copper bond joint.

## VI. CONCLUSION

In order to achieve better cooling effect, we proposed an advanced flexible multiflow path fixture cooling method for blade additive manufacturing repair. Through problem analysis, theoretical modeling, numerical analysis and experiment, the conclusions are as follows:

(1) Due to the original structural limitations of the fixture base cooling method, the heat exchange effect of the fluid is not fully utilized; regardless of whether $V$, $T$ or $L$ is changed, the cooling effect does not change significantly. Using the flexible flow-path cooling method, the initial temperature of the fixture can be quickly reduced, and the fixture can be cooled to an initial temperature equal to the temperature of the fluid, forming a steady-state cooling conduction with the fluid.

(2) The fluid closest to the contact surface in the flow path is obviously involved in heat transfer. The isothermal surface analysis results show that when the heat source moves directly above the copper bond, fluids of adjacent copper bonds can participate in the heat transfer. When the heat source moves directly above the corner point of the copper bond, fluids with two copper bonds on each side participate in heat exchange.

(3) Compared with the cooling effect of the fixture base cooling method with a single flow path, the flexible multiflow path cooling method can reduce the cross-sectional temperature of the weld seam by 140∼160 °C, and the significant decrease in the temperature of the contact surface between the fixture and the test piece also shows that the new method can achieve faster heat conduction.

(4) The comparison of the cooling effect at different flow rates shows that with the increase in the flow rate, the temperature of the weld cross-section and the fixture can continue to decrease. However, the increase in the flow rate will cause an increase in the pipeline pressure and resistance and turbulent resonance problems. Considering all of the influencing factors comprehensively, under the existing processing technology conditions, a flow rate of 2 L/min can achieve a better cooling effect.

## EXPECTATION

Due to the limitations of processing technology, the pressure resistance and sealing of the fixture prototype need to be further improved. Further study will focus on the feasibility of 3D printing or precision casting technology for the manufacturing of the flexible flow path fixture and improved processing technology to achieve loading on the welding system, which is expected to further improve the cooling effect.

## REFERENCES

[1] G. Miao, S. Dai, P. Jia, and D. Wang, "Heat transfer modeling and cooling method for aeroengine blade MPAW repair," *Trans. China Weld. Inst.*, vol. 40, no. 7, pp. 24–30 and 162, Jul. 2019.

[2] W. Qu and I. Mudawar, "Experimental and numerical study of pressure drop and heat transfer in a single-phase micro-channel heat sink," *Int. J. Heat Mass Transf.*, vol. 45, no. 12, pp. 2549–2565, Jun. 2002.

[3] H. H. Wu, Y. Y. Hsiao, H. S. Huang, and P. H. Tang, "A practical plate-fin heat sink model," *Appl. Thermal Eng.*, vol. 31, no. 5, pp. 984–992, May 2011.
[4] S. Dai, M. Gong, L. Wang, and T. Wang, "Research on cooling method in surfacing repair process of aero compressor blade," *Math. Problems Eng.*, vol. 2020, Feb. 2020, Art. no. 1208313.
[5] N. Jalili, H. B. Tabrizi, and M. M. Hosseini, "Experimental and numerical study of simultaneous cooling with $CO_2$ gas during friction stir welding of Al-5052," *J. Mater. Process. Technol.*, vol. 237, pp. 243–253, Nov. 2016.
[6] M. Imam, R. Ueji, and H. Fujii, "Effect of online rapid cooling on microstructure and mechanical properties of friction stir welded medium carbon steel," *J. Mater. Process. Technol.*, vol. 230, pp. 62–71, Apr. 2016.
[7] H. Hamatani, Y. Miyazaki, T. Otani, and S. Ohkita, "Minimization of heat-affected zone size in welded ultra-fine grained steel under cooling by liquid nitrogen during laser welding," *Mater. Sci. Eng.: A*, vol. 426, nos. 1–2, pp. 21–30, Jun. 2006.
[8] S. G. K. Manikandan, D. Sivakumar, K. Prasad Rao, and M. Kamaraj, "Microstructural characterization of liquid nitrogen cooled alloy 718 fusion zone," *J. Mater. Process. Technol.*, vol. 214, no. 12, pp. 3141–3149, Dec. 2014.
[9] S. G. K. Manikandan, D. Sivakumar, and K. P. Rao, "Effect of weld cooling rate on Laves phase formation in Inconel 718 fusion zone," *J. Mater. Process. Technol.*, vol. 214, no. 2, pp. 358–364, Feb. 2014.
[10] L. Biswal, S. Chakraborty, and S. K. Som, "Design and optimization of single-phase liquid cooled microchannel heat sink," *IEEE Trans. Compon. Packag. Technol.*, vol. 32, no. 4, pp. 876–886, Dec. 2009.
[11] J. Guisheng, "Optimization design of water-cooled heat sink applied to large-capacity power electronic equipment," *J. Mech. Eng.*, vol. 46, no. 2, pp. 99–105, Feb. 2010.
[12] S. J. S. Xiaozhe, "Effect of cooling conditions on microstructure and properties of 2219 aluminum alloy FSW joints," *Hot Work. Technol.*, vol. 47, no. 17, pp. 25–29 and 35, Sep. 2018.
[13] S. Kangning, C. Yi, and L. Zhimin, "Influence of different cooling methods on microstructure and mechanical properties of 7 series aluminum alloy MIG welded joints," *Hot Work. Technol.*, vol. 47, no. 5, pp. 54–57, May 2018.
[14] W. Fan, S. Ao, Y. Huang, W. Liu, Y. Li, Y. Feng, Z. Luo, and B. Wu, "Water cooling keyhole gas tungsten arc welding of HSLA steel," *Int. J. Adv. Manuf. Technol.*, vol. 92, no. 6, pp. 2207–2216, Jun. 2017.
[15] W. Peng, "Buckling distortion of laser welded thin plates and its control by dynamic cooling," *Trans.-China Weld. Inst.*, vol. 27, no. 9, pp. 99–102, Sep. 2006.
[16] J. Wang, Y. Li, X. Liu, C. Shen, H. Zhang, and K. Xiong, "Recent active thermal management technologies for the development of energy-optimized aerospace vehicles in China," *Chin. J. Aeronaut.*, 2020, doi: 10.1016/j.cja.2020.06.021.
[17] J.-X. Wang, W. Guo, K. Xiong, and S.-N. Wang, "Review of aerospace-oriented spray cooling technology," *Prog. Aerosp. Sci.*, vol. 116, Jul. 2020, Art. no. 100635.
[18] J.-X. Wang, Y.-Z. Li, J.-X. Li, C. Li, Y. Zhang, and X.-W. Ning, "A gas-atomized spray cooling system integrated with an ejector loop: Ejector modeling and thermal performance analysis," *Energy Convers. Manage.*, vol. 180, pp. 106–118, Jan. 2019.
[19] J.-X. Wang, Y.-Z. Li, M.-L. Zhong, and H.-S. Zhang, "Investigation on a gas-atomized spray cooling upon flat and micro-structured surfaces," *Int. J. Thermal Sci.*, vol. 161, Mar. 2021, Art. no. 106751.
[20] S. Jiamin, H. Jing, and D. De'an, "Numerical simulation of the influence of forced cooling on the temperature field of electroslag welding joint," *Trans. China Weld. Inst.*, vol. 37, no. 1, pp. 63–66 and 132, Jan. 2016.
[21] I. Khalil, R. Hayes, Q. Pratt, C. Spitler, and D. Codd, "Experimental and numerical modeling of heat transfer in directed thermoplates," *Int. J. Heat Mass Transf.*, vol. 123, pp. 89–96, Aug. 2018.
[22] M. Sosnowski, J. Krzywanski, and R. Scurek, "A fuzzy logic approach for the reduction of mesh-induced error in CFD analysis: A case study of an impinging jet," *Entropy*, vol. 21, no. 11, p. 1047, Oct. 2019.
[23] M. Sosnowski, "Evaluation of heat transfer performance of a multi-disc sorption bed dedicated for adsorption cooling technology," *Energies*, vol. 12, no. 24, p. 4660, Dec. 2019.
[24] H. G. Sun and W. J. Huo, "Aeroengine turbine blade repair technology," *Aviation Maintenance*, vol. 6, pp. 12–13, Jun. 2001.
[25] R. J. Bai and L. G. Zhang, "Turbine blade repairing and its market analysis," *Aeronaut. Manuf. Technol.*, vol. 12, pp. 37–40, Dec. 2002.
[26] W. Hao, "Method and implementation of remanufacturing and repair of aircraft engine damaged blade," *Acta Aeronautica et Astronautica Sinica*, vol. 37, no. 3, pp. 1036–1048, Mar. 2016.
[27] M. Baruah and S. Bag, "Influence of heat input in microwelding of titanium alloy by micro plasma arc," *J. Mater. Process. Technol.*, vol. 231, pp. 100–112, May 2016.
[28] L. Haihua, C. Haojie, L. Wenji, W. Tianqi, and Y. Jianfeng, "Numerical analysis of flow-thermal coupling in micro-plasma welding pool of thin-wall part," *China Weld.*, vol. 27, no. 2, pp. 13–18, Feb. 2018.
[29] S. Dai, M. Gong, L. Wang, and T. Wang, "Numerical analysis and experimental verification of optimum heat input in additive manufacturing of aero ultrathin blade," *Math. Problems Eng.*, vol. 2021, Jan. 2021, Art. no. 1648075.
[30] G. Miao, "Research on optimal heat input for blade repair of aero compressor," *Trans. The China Weld. Inst.*, vol. 41, no. 8, pp. 39–47, Aug. 2020.
[31] S. Dai, D. Wang, H. Zhang, S. Li, and Z. Wang, "Thermal contact resistance between aero engine compressor blade and flexible fixture," *J. Thermal Sci.*, May 2020.

**MIAO GONG** received the M.Sc. degree from the Civil Aviation University of China, Tianjin, China, in 2010, and the Ph.D. degree from the Hebei University of Technology, Tianjin, in 2020. He is currently an Associate Research Fellow with the Civil Aviation University of China. His main research interests include research and development of civil aviation special equipment and systems.

**SHIJIE DAI** received the M.Sc. degree from the Hebei University of Technology, Tianjin, China, in 1999, and the Ph.D. degree from the Harbin Institute of Technology, Harbin, China, in 2003. He is currently a Professor with the Hebei University of Technology and a member of the Tianjin Automation Technology and Application Research Association. His main research interests include machine vision and robotic systems integration.

**LIWEN WANG** received the M.Sc. and Ph.D. degrees from the Harbin Institute of Technology, Harbin, China, in 1989 and 1995, respectively. He is currently a Professor with the Civil Aviation University of China. His main research interests include civil aviation ground special equipment and fluid transmission and control. He is also a Special Expert on CAAC, a Director of the Chinese Society of Aeronautics, and a member of the China Society of Mechanical Engineering.

**TAO WANG** received the M.Sc. and Ph.D. degrees from Tianjin University, Tianjin, China, in 2005 and 2008, respectively. He is currently a Professor with the Civil Aviation University of China. His main research interests include additive manufacturing of aero blades and laser deposition. He is a member of the Machine Tool Professional Committee of China Machine Production Engineering Society and the Online Testing Committee of China Metrology Society.